 CMC, vol.24, no.1, pp.61-104, 2011

A Simple Procedure to Develop Efficient & Stable Hybrid/Mixed Elements, and Voronoi Cell Finite Elements for Macro- & Micromechanics

L. Dong[1] **and S. N. Atluri**[2]

Abstract: A simple procedure to formulate efficient and stable hybrid/mixed finite elements is developed, for applications in macro- as well as micromechanics. In this method, the strain and displacement field are independently assumed. Instead of using two-field variational principles to enforce both equilibrium and compatibility conditions in a variational sense, the independently assumed element strains are related to the strains derived from the independently assumed element displacements, at a finite number of collocation points within the element. The element stiffness matrix is therefore derived, by simply using the principle of minimum potential energy. Taking the four-node plane isoparametric element as an example, different hybrid/mixed elements are derived, by adopting different element strain field assumptions, and using different collocation points. These elements are guaranteed to be stable. Moreover, the computational efficiency of these elements is far better than that for traditional hybrid/mixed elements, or even better than primal finite elements, because the strain field is expressed analytically as simple polynomials (whereas, in isoparametric displacement-based element, the strain field is far more complicated), with nodal displacements as unknowns. The essential idea is thereafter extended to Voronoi cell finite elements, for micromechanical analysis of materials. Neither these four-node hybrid/mixed elements nor the Vonroni cell finite elements need to satisfy the equilibrium conditions a priori, making them suitable for extension to geometrically nonlinear and dynamical analyses. Various numerical experiments are conducted using these new elements, and the results are compared to those obtained by using traditional hybrid/mixed elements and primal finite elements. Performances of the different elements are compared in terms of efficiency, stability, invariance, locking, sensitivity to mesh distortion, and convergence rates.

[1] Department of Civil & Environmental Engineering, University of California, Irvine, Email: leitingd@uci.edu

[2] Center for Aerospace Research & Education, University of California, Irvine

Keywords: hybrid/mixed finite elements, efficiency, stability, LBB conditions, variational principle, invariance, locking, collocation, Voronoi cell, RBF

1 Introduction

Primal and complementary finite element methods are widely accepted and applied for computer modeling of physical problems, because of their simplicity and efficiency. However, disadvantages of these methods are also well-known, such as locking phenomena in problems which involve constraints, difficulty to satisfy continuity requirements (especially in plates and shells), sensitivity to mesh distortion, etc. Carefully formulated finite elements based on multi-field assumptions, on the other hand, can mitigate or even resolve such problems. Thus, since its early development in 1960s, numerous formulations of hybrid/mixed finite element have been proposed and applied to various physical problems.

The original version of the hybrid stress elements developed in [Pian (1964)] were based on the modified principle of minimum complementary energy, using "a priori equilibrated" stress field in each element, and continuous displacement field along element edges. Besides its better element performance, the great advantage of this method is recognized to be its ability to satisfy higher-order continuity requirements. However, for geometrical nonlinear and dynamical problems, it is more convenient to develop hybrid/mixed finite elements based on "a posteriori equilibrated" stress field, and continuous displacement field inside each element, using Reissner's variational principle, as in [Atluri (1975); Atluri, Tong and Murakawa (1983); Cai, Paik and Atluri (2009); Cai, Paik and Atluri (2009); Cai, Paik and Atluri (2010); Cai, Paik and Atluri (2010); Zhu, Cai, Paik and Atluri (2010)]. Other hybrid/mixed finite element methods were also formulated based on the assumptions of stress and incompatible displacement field using modified Reissner's Principle by [Pian and Wu (1988)], assumptions of displacement, stress and strain field using Hu-Washizu principle by [Atluri (1975); Atluri, Tong and Murakawa (1983); Tang, Chen and Liu (1984)], etc.

Besides their applications in two-dimensional and three-dimensional solid mechanics, hybrid/mixed finite element methods also demonstrated their advantages in other types of physical problems. For example, [Lee and Pian (1978), Cai, Paik and Atluri (2009); Cai, Paik and Atluri (2009); Cai, Paik and Atluri (2010); Cai, Paik and Atluri (2010); Zhu, Cai, Paik and Atluri (2010)] developed locking-free hybrid/mixed finite elements for modeling plates and shells. [Bratianu and Atluri (1983); Ying and Atluri (1983)] developed stable mixed finite elements for Stokes flows, which eliminate incompressibility locking without resolving to selective reduced-order integrations. [Pian and Mau (1972); Cazzani, Garusi, Tralli and Atluri (2005)] developed different hybrid element formulations to analyze lam-

inated composite plates. [Ghosh and Mallett (1994); Ghosh, Lee and Moorthy (1995)] developed Voronoi cell finite elements and applied them to multi-scale analysis of structures composed of heterogeneous materials.

However, in spite of their widely recognized advantages, there are essentially two major drawbacks that have been limiting the engineering applications of hybrid/mixed finite elements. One is the increased computational burden caused by matrix inversion for each and every element, and the need to generate two different element matrices (**H** and **G**) through integrations over the element, in the process of developing the element stiffness matrix. The other is the questionable stability of finite element solutions. Matrix inversion is hard to avoid as long as multi-field variational principles are used for element derivation. Regarding stability, [Babuska (1973); Brezzi (1974)] analyzed the existence, uniqueness, stability and convergence of saddle point problems and established the so-called LBB conditions. Inability to satisfy LBB conditions in general would plague the solvability and stability of hybrid/mixed finite element equations. [Rubinstein, Punch and Atluri (1983); Punch and Atluri (1984); Xue, Karlovitz and Atluri (1985)] used sophisticated group theory to develop guidelines for selecting least-order stress interpolations, from which stable and invariant finite elements satisfying LBB conditions can be formulated. [Pian and Chen (1983)] also proposed to choose stress interpolations by matching each stress/strain mode to stress/strain modes derived from non-rigid body displacement modes.

When multi-field variational principles are used to derive hybrid/mixed elements, one has to deal with the additional computational burden, and select field assumptions in a complicated manner to satisfy complicated LBB conditions. In this paper, we try to develop hybrid/mixed elements without using multi-field variational principles. The essential idea of this approach is to relate independently assumed strains to nodal displacements in a simple way, without using multi-field variational principles. Such a relation can be easily established by enforcing the compatibility of independently assumed strains, and the strains derived from independently assumed displacements, at a finite number of collocation points within the element. The element stiffness matrix can thereafter be easily formulated using the principle of minimum potential energy. Because no Lagrangian multipliers are involved, this new approach is not plagued by LBB conditions. Moreover, because strains, which are analytically expressed in terms of nodal displacements, are simple polynomials, the stiffness matrix can be derived using very few quadrature points or even analytically. Thus, this approach is expected to be not only stable but also computationally efficient. Finally, the essential idea of this approach is extended to develop Voronoi cell finite elements, leading to simple elements suitable for not only linear static, but also nonlinear and dynamical problems, especially in study-

ing the micromechanics of materials.

This paper is organized as follows. In section 2, some basics of linear elasticity and variational principles are reviewed, and their relations to finite element methods are discussed. In section 3, we present a family of hybrid/mixed elements, which are developed using a conventional two-field variational principle, denoted as HMFEM1. We also illustrate why these elements are computationally inefficient, and are plagued by LBB conditions. In section 4, we present a simple class of hybrid/mixed elements—HMFEM2, which is efficient and are not plagued by LBB conditions. In section 5, we extend the essential idea of HMFEM2 to Voronoi cell finite elements. In Section 6, we evaluate the performance of different elements by conducting numerical experiments. Finally, in section 7, we present some concluding remarks.

2 Basics of Linear Elasticity and Variational Principle

Consider a linear elastic solid undergoing infinitesimal deformation. Cartesian coordinates x_i identify material particles in the solid. $\sigma_{ij}, \varepsilon_{ij}, u_i$ are components of stress tensor, strain tensor and displacement vector respectively. $\overline{f}_i, \overline{u}_i, \overline{t}_i$ are components of prescribed body force, boundary displacement and boundary traction vector. S_u, S_t are displacement boundary and traction boundary of the domain Ω. We use $()_{,i}$ to denote partial differentiation with respect to x_i. The governing static equilibrium, constitutive, and compatibility equations, and boundary conditions can be written as:

$$\sigma_{ij,j} + \overline{f}_i = 0;\ \sigma_{ij} = \sigma_{ji} \text{ in } \Omega \tag{1}$$

$$\sigma_{ij} = \frac{\partial W}{\partial \varepsilon_{ij}};\ W \equiv \frac{1}{2} E_{ijkl}\varepsilon_{ij}\varepsilon_{kl} \text{ in } \Omega \text{ for a linear elastic solid} \tag{2}$$

$$\varepsilon_{ij} = \frac{1}{2}(u_{i,j} + u_{j,i}) \equiv u_{(i,j)} \text{ in } \Omega \tag{3}$$

$$n_j \sigma_{ij} = \bar{t}_i \text{ at } S_t \tag{4}$$

$$n_j \sigma_{ij} = \bar{t}_i \text{ at } S_t \tag{5}$$

If constitutive equations (2) are satisfied a priori, and if we consider differentiable symmetric stresses, differentiable displacements and only conservative loading, Reissner's variational principle in [Reissner (1950)] states that (1)(3)(4)(5) can be derived from the stationarity conditions of the following two-field functional:

$$\begin{aligned} \pi_1(\sigma_{ij}, u_i) = &\int_\Omega \left[-W_c(\sigma_{ij}) + \sigma_{ij} u_{(i,j)} - \overline{f}_i u_i\right] d\Omega \\ &- \int_{S_t} \bar{t}_i u_i dS - \int_{S_u} t_i (u_i - \overline{u}_i) dS \end{aligned} \tag{6}$$

where W_c is the complementary energy density function, which is obtained through the contact transformation

$$W_c(\sigma_{ij}) = \sigma_{ij}\varepsilon_{ij} - W(\varepsilon_{ij}) \tag{7}$$

such that

$$\frac{\partial W_c}{\partial \sigma_{ij}} = \varepsilon_{ij} \tag{8}$$

On the other hand, if we treat both ε_{ij} and u_i as independent variables as illustrated in the monograph [Atluri (2005)], instead of σ_{ij} and u_i as in Reissner's variational principle, we obtain another variational principle from the stationarity conditions of the following two-field functional:

$$\begin{aligned}\pi_2(\varepsilon_{ij}, u_i) = &\int_\Omega \left[W(\varepsilon_{ij}) - \frac{\partial W}{\partial \varepsilon_{ij}}(\varepsilon_{ij} - u_{(i,j)}) - \overline{f}_i u_i \right] d\Omega \\ &- \int_{S_t} \overline{t}_i u_i dS - \int_{S_u} t_i (u_i - \overline{u}_i) dS\end{aligned} \tag{9}$$

such that

$$\begin{aligned}\delta\pi_2 =& 0 \\ =& -\int_\Omega \left\{ \left[\left(\frac{\partial W}{\partial \varepsilon_{ij}} \right)_{,j} + \overline{f}_i \right] \delta u_i + (\varepsilon_{ij} - u_{(i,j)}) \delta \frac{\partial W}{\partial \varepsilon_{ij}} \right\} d\Omega \\ &+ \int_{S_t} (t_i - \overline{t}_i) \delta u_i dS - \int_{S_u} (u_i - \overline{u}_i) \delta t_i dS\end{aligned} \tag{10}$$

which can be seen to lead to the Euler-Lagrange equations:

$$\left(\frac{\partial W}{\partial \varepsilon_{ij}} \right)_{,j} + \overline{f}_i = 0 \text{ in } \Omega \tag{11}$$

$$\varepsilon_{ij} = u_{(i,j)} \text{ in } \Omega \tag{12}$$

$$u_i = \overline{u}_i \text{ at } S_u,\ t_i = \overline{t}_i \text{ at } S_t \tag{13}$$

In addition, $\frac{\partial W}{\partial \varepsilon_{ij}} = \frac{\partial W}{\partial \varepsilon_{ji}}$ are guaranteed by the definition of W.

We note the philosophical difference between Reissner's variational principle involving σ_{ij} and u_i as in (6) and the modified principle involving ε_{ij} and u_i as in (9). The present principle involving independent fields ε_{ij} and u_i is of fundamental interest of constructing finite elements. In the mesh-based finite element method, a

compatible assumed displacement field for an element, involving nodal shape functions, is not necessarily a complete polynomial, and the strain field derived from such a displacement field is even less complete. The incomplete strains are locked together, thus leading to the well-known locking phenomena. However, independent assumptions of ε_{ij} and u_i would provide the flexibility to choose a strain field which eliminates the locking phenomena. In this sense, independent assumptions of ε_{ij} and u_i are more straight-forward than independent assumptions of σ_{ij} and u_i in order to avoid locking phenomena.

Moreover, when the domain Ω is discretized into subdomains Ω_m (finite elements) with boundaries $\partial\Omega_m$, each subdomain boundary can be divided into S_{um}, S_{tm}, ρ_m, which are intersections with S_u, S_t and other subdomains respectively. Then, in addition to satisfying (1)(2)(3) in each Ω_m, satisfying (4)(5) at S_{um}, S_{tm}, displacement compatibility and traction reciprocity conditions at each inter-subdomain boundary should be considered:

$$u_i^+ = u_i^- \text{ at } \rho_m \tag{14}$$

$$(n_j\sigma_{ij})^+ + (n_j\sigma_{ij})^- = 0 \text{ at } \rho_m \tag{15}$$

In general, these conditions do not need to be satisfied a priori, which leads to different modified variational principles, as summarized in [Xue, Karlovitz, Atluri (1985)]. For example, if we consider assumed "a priori equilibrated stress field" and inter-element continuous displacement field with (1)(2)(4)(14) satisfied, (3)(5)(15) can be derived from the stationarity conditions of the following functional, which is often referred to as the modified principle of minimum complementary energy:

$$\pi_3(\sigma_{ij}, u_i) = \sum_m \left\{ \int_{\Omega m} W_c(\sigma_{ij}) d\Omega - \int_{\partial\Omega_m} t_i u_i dS + \int_{S_{tm}} \bar{t}_i u_i dS \right\} \tag{16}$$

In another way, if we consider assumed strain field and continuous displacement field which satisfy (4)(14) and constitutive equation (2), then (1)(3)(5)(15) can be derived by the stationarity conditions of the following functional:

$$\pi_4(\varepsilon_{ij}, u_i) = \sum_m \left\{ \int_{\Omega m} \left[W(\varepsilon_{ij}) - \frac{\partial W}{\partial \varepsilon_{ij}} \left(\varepsilon_{ij} - u_{(i,j)} \right) - \overline{f}_i u_i \right] d\Omega - \int_{S_{tm}} \bar{t}_i u_i dS \right\} \tag{17}$$

Variational principle (16) and (6) are among those originally used to derive hybrid/mixed finite elements, as in [Pian (1964); Atluri (1975); Atluri, Tong and Murakawa (1983)]. However, it is well-known that the two-field variational principle of Reissner (6), and the modified principle of minimum complementary energy (16) involve Lagrangian multipliers, which necessitate the selection of σ_{ij} and $u_i$to satisfy the so-called LBB conditions—conditions which have plagued the successful

development of hybrid/mixed finite element methods. Likewise, the development of finite elements based on two-field (ε_{ij} and u_i) principle of (9) or (17) is also plagued by LBB conditions.

On the other hand, if we consider a compatible displacement field which satisfies (2)(3) (4)(14) a priori , (1)(5)(15) can be derived by the stationarity conditions of the following primitive-field variational principle:

$$\pi_5(u_i) = \sum_m \left\{ \int_{\Omega m} \left[W(\varepsilon_{ij}(u_k)) - \overline{f}_i u_i \right] d\Omega - \int_{S_{tm}} \bar{t}_i u_i dS \right\} \tag{18}$$

This primitive-field variational principle, which is often referred to as the principle of minimum potential energy, can be used to develop mesh-based primal finite elements, based on assumption of displacement field only. These primal finite elements suffer from the well-known locking phenomena as described previously. However, because no Lagrangian multiplier or saddle point problems are involved, these displacement-based primal finite elements are not plagued by the so-called LBB conditions.

3 Hybrid/Mixed Finite Elements Using a Two-field Variational Principle

Consider a general isoparametric element with the following interpolations:

$$x_i = \sum_n x_i^{(n)} N^{(n)}(\xi^\gamma) \tag{19}$$

$$u_i = \sum_n u_i^{(n)} N^{(n)}(\xi^\gamma) \tag{20}$$

where x_i are the global Cartesian coordinates, and ξ^γ are the local non-dimensional element curvilinear coordinates. The subscripts indicate Cartesian coordinates, and the superscripts indicate node numbers. In general, $N_i^{(n)}(\xi^\gamma)$ should be polynomials which are complete to a certain order. With this assumption, the inter-element displacement compatibility is easily satisfied a priori, and the displacement boundary condition can also be satisfied a priori by prescribing nodal displacements on the displacement boundary.

On the other hand, strain field in this element can be assumed independently as:

$$\varepsilon_{ij} = \varepsilon_{ij}(\xi^\gamma, \boldsymbol{\alpha}) \tag{21}$$

where $\varepsilon_{ij}(\xi^\gamma, \boldsymbol{\alpha})$ are usually defined as simple polynomials which are complete to a certain order. $\boldsymbol{\alpha}$ is a vector containing undetermined parameters.

We denote, with matrix and vector notation, in each Ω_m and at $\partial\Omega_m$:

$$\mathbf{u} = \mathbf{N}(\xi^\gamma)\mathbf{q} \tag{22}$$

$$\mathbf{u}_{(i,j)} = \mathbf{B}(\xi^\gamma)\mathbf{q} \tag{23}$$

$$\boldsymbol{\varepsilon} = \mathbf{A}(\xi^\gamma)\boldsymbol{\alpha} \tag{24}$$

$$\boldsymbol{\sigma} = \mathbf{D}\boldsymbol{\varepsilon} \tag{25}$$

$$\mathbf{t} = \mathbf{n}\boldsymbol{\sigma} \tag{26}$$

Using the two field variational principle (17), we obtain:

$$\begin{aligned} &\delta\pi_4(\boldsymbol{\alpha},\mathbf{q}) = 0 \\ &= \delta\sum_m \left(-\frac{1}{2}\boldsymbol{\alpha}^T\mathbf{H}\boldsymbol{\alpha} + \mathbf{q}^T\mathbf{G}^T\boldsymbol{\alpha} - \mathbf{q}^T\mathbf{Q}\right) \\ &= \sum_m \left(-\delta\boldsymbol{\alpha}^T\mathbf{H}\boldsymbol{\alpha} + \delta\mathbf{q}^T\mathbf{G}^T\boldsymbol{\alpha} + \delta\boldsymbol{\alpha}^T\mathbf{G}\mathbf{q} - \delta\mathbf{q}^T\mathbf{Q}\right) \end{aligned} \tag{27}$$

$$\mathbf{G} = \int_{\Omega m} \mathbf{A}^T(\xi^\gamma)^T\mathbf{D}\mathbf{B}(\xi^\gamma)d\Omega \tag{28}$$

$$\mathbf{H} = \int_{\Omega m} \mathbf{A}^T(\xi^\gamma)\mathbf{D}\mathbf{A}(\xi^\gamma)d\Omega \tag{29}$$

$$\mathbf{Q} = \int_{\Omega m} \mathbf{N}^T(\xi^\gamma)\bar{\mathbf{f}}d\Omega + \int_{Stm} \mathbf{N}^T(\xi^\gamma)\bar{\mathbf{t}}dS \tag{30}$$

Because $\delta\boldsymbol{\alpha}$ is totally arbitrary in each Ω_m, while $\delta\mathbf{q}$ need to satisfy inter-element displacement compatibility (14) and displacement boundary condition (4), (27) leads to:

$$\mathbf{G}\mathbf{q} - \mathbf{H}\boldsymbol{\alpha} = 0 \tag{31}$$

$$\sum_m \left(\delta\mathbf{q}^T\mathbf{G}^T\boldsymbol{\alpha} - \delta\mathbf{q}^T\mathbf{Q}\right) = 0 \tag{32}$$

Therefore finite element equations are formulated as:

$$\sum_m \left(\delta\mathbf{q}^T\mathbf{K}^\mathbf{e}\mathbf{q} - \delta\mathbf{q}^T\mathbf{Q}\right) = \sum_m \left(\delta\mathbf{q}^T\mathbf{G}^T\mathbf{H}^{-1}\mathbf{G}\mathbf{q} - \delta\mathbf{q}^T\mathbf{Q}\right) = 0 \tag{33}$$

After applying the displacement boundary condition, (33) can be solved for nodal displacements, and the stress and strain fields can be calculated as:

$$\boldsymbol{\varepsilon} = \mathbf{A}(\xi^\gamma)\mathbf{H}^{-1}\mathbf{G}\mathbf{q} \tag{34}$$

$$\boldsymbol{\sigma} = \mathbf{DA}(\xi^{\gamma})\mathbf{H}^{-1}\mathbf{Gq} \tag{35}$$

We denote this hybrid/mixed finite element method as HMFEM1.

As seen in (33), one major drawback of HMFEM1 is its computational inefficiency. One has to compute matrices $\mathbf{H}$ and $\mathbf{G}$ using numerical quadrature over each element, and carry out the matrix inversion of $\mathbf{H}$ for each and every element. This situation exists almost for every hybrid/mixed finite element, as long as multi-field variational principles are used.

Another drawback of HMFEM1 is that careful attention should be paid to the question of how to select the independent strain field in order to obtain a stable element performance. [Babuska (1973); Brezzi (1974)] studied general saddle-point problems or problems involving Lagrangian multipliers, and established so-called LBB conditions. Because the derivation of HMFEM1 involves Lagrangian multiplier $\frac{\partial W}{\partial \varepsilon_{ij}}$, as seen in the two-field principle (17), the solvability and stability of HMFEM1 is governed by LBB conditions.

For linear elastic solid mechanics, if we define:

$$\begin{aligned}
V &= \{v_i \in H^1(\Omega_m), v_i^+ = v_i^- \text{ at } \rho_m,\ v_i = 0 \text{ at } S_{um}, \forall m\} \\
T &= \{\tau_{ij} \in \mathrm{H}^1(\Omega_m), \forall m\} \\
V_h &= \{v_i \in V, \{v_i\} = \mathbf{N}(\xi^{\gamma})\mathbf{p}, \text{in } \Omega_m, \forall m\} \\
T_h &= \{\tau_{ij} \in T, \{\tau_{ij}\} = \mathbf{A}(\xi^{\gamma})\boldsymbol{\alpha}, \text{in } \Omega_m, \forall m\} \\
Ker(\mathbf{B}) &= \{\varepsilon_{ij} \in T_h, \sum_m \int_{\Omega_m} \sigma_{ij}(\varepsilon_{kl}) v_{(i,j)} d\Omega = 0, \forall v_i \in V_h\}
\end{aligned} \tag{36}$$

LBB conditions states that:

$$\exists \alpha > 0, \text{ such that } W_c(\sigma_{ij}(\varepsilon_{kl})) \geq \alpha \left\|\varepsilon_{ij}\right\|_{T_h}^2, \forall \varepsilon_{ij} \in Ker(\mathbf{B}) \tag{37}$$

$$\exists \beta > 0, \text{ such that } \inf_{v_i \in V_h} \sup_{\varepsilon_{ij} \in T_h} \frac{\sum_m \int_{\Omega_m} \sigma_{ij}(\varepsilon_{kl}) v_{(i,j)} d\Omega}{\left\|\varepsilon_{ij}\right\|_{T_h} \left\|v_i\right\|_{V_h}} \geq \beta \tag{38}$$

If one can find such positive numbers α, β, the finite element formulation has a unique and stable solution. Moreover, if α, β do not depend on mesh size h, then the "uniform stability" and convergence are established. For a linear elastic solid with positive-definite material property, one can readily find that condition (37) is always satisfied. Therefore, (38) becomes the key condition governing the performance of this hybrid/mixed finite element method. By noticing that the rigid body displacement is prevented by displacement boundary condition, a sufficient condition to ensure such a positive β exists as in (38) are found, as summarized in [Xue,

Karlovitz, Atluri (1985)]:

$$\sup_{\varepsilon_{ij}\in T_h}\int_{\Omega_m}\sigma_{ij}^{m}(\varepsilon_{kl})v_{(i,j)}^{md}d\Omega>0,\forall v_{(i,j)}^{md},v_i\in V_h \tag{39}$$

In (39), superscript *md* denotes non-rigid body modes in each element. It should be noted that (39) is not a sufficient condition for "uniform stability" and convergence, because whether or not β is uniformly bounded from below independent of h has to be checked separately. But (39) guarantees that a unique and stable solution can be found, which is highly desired in engineering applications. Furthermore, it can be seen that (39) has a strong physical meaning, that for every non-rigid body displacement mode in each element, there should be at least one independent assumed strain mode, so that the derived "mixed strain energy" is positive. This condition is frequently considered as free of zero-energy/kinematic/spurious modes in a mechanics point of view, as seen in [Bicanic and Hinton (1979); Rubinstein, Punch and Atluri (1983)]. We use matrix notation to write (39) as:

$$\sup_{\boldsymbol{\alpha}}\int_{\Omega_m}\boldsymbol{\alpha}^T\mathbf{A}^T(\xi^\gamma)\mathbf{D}\mathbf{B}(\xi^\gamma)\mathbf{q}^{md}d\Omega=\sup_{\boldsymbol{\alpha}}\boldsymbol{\alpha}^T\mathbf{G}\mathbf{q}^{md}>0,\ \forall\mathbf{q}^{md} \tag{40}$$

Since r rigid-body mode $\mathbf{q}^r$ are definitely in the null space of $\mathbf{G}$, an equivalent condition to (40) can be readily found as:

$$rank(\mathbf{G})=n_{dof}-r \tag{41}$$

where n_{dof} is the number of nodal degree of freedoms of the element. (41) is frequently referred to as condition of rank-sufficiency of derived element. We notice that to ensure (41) beforehand in element formulation level is difficult, where selecting at least $n_{dof}-r$ independent strain modes is merely a necessary condition. In [Rubinstein, Punch and Atluri (1983); Punch and Atluri (1984)], symmetric group theory was for the first time utilized to prevent element rank deficiency (in a case of assumed σ_{ij} and v_i). In this method, assumed σ_{ij} and $v_{(i,j)}$ are firstly decomposed into invariant irreducible spaces using symmetric group theory. In terms of these irreducible representations, the matrix corresponding to $\int_{\Omega_m}\sigma_{ij}^{m}v_{(i,j)}^{md}d\Omega$ is shown to be "quasi-diagonal". Thus, one can pick least-order modes σ_{ij} to ensure that the derived element is stable. Although this method can be also applied to HMFEM1, based on assumption of ε_{ij} and u_i, its application in engineering is limited by the mathematical sophistication and complexity of group theory. [Pian and Chen (1983)] also proposed a method of suppressing zero-energy modes by matching each assumed stress/strain mode to $\sigma_{ij}(q^{md})$ or $\varepsilon_{ij}(q^{md})$, without considering the invariance of derived elements. However, no matter which method one

chooses to use, we see that because of LBB conditions, stress or strain field cannot be arbitrarily chosen, careful and complicated analysis has to be conducted in order to ensure the stability of solution, which is especially complicated for three-dimensional higher-order elements.

4 A Simple Method to Develop Efficient, Stable and Invariant Hybrid/Mixed Finite Elements:

4.1 Essential Idea and Basic Formulation

We notice that the two major drawbacks of HMFEM1 are both due to the fact that a two-field variational principle (17) is used for element derivation: such a varational principle leads to the necessity for the evaluation of $\mathbf{H}^{-1}$ for each and every element, and involves Lagrangian multiplier $\frac{\partial W}{\partial \varepsilon_{ij}}$. Therefore, we step out of this stencil and instead seek other ways to relate independently assumed strain field in each element to nodal displacements. We notice such a relation can be easily established by enforcing compatibility of independently assumed strains, and strains derived from independently assumed displacements, at several pre-selected collocation points $\xi^{\gamma k},\ k = 1,2,...,M$, which leads to:

$$\varepsilon_{ij}(\xi^{\gamma k}, \boldsymbol{\alpha}) = \varepsilon_{ij}(\xi^{\gamma k}, \mathbf{q}) \tag{42}$$

where $\varepsilon_{ij}(\xi^{\gamma k}, \boldsymbol{\alpha}), \varepsilon_{ij}(\xi^{\gamma k}, \mathbf{q})$ are the assumed strain field, and the strain field derived from assumed displacement field respectively, at point $\xi^{\gamma k}$. It should be noted that, one does not need to collocate every strain component at each point $\xi^{\gamma k}$. For example, for two-dimensional problems, one can collocate ε_{11} at points $\xi^{\gamma k_{11}}$, collocate ε_{22} at points $\xi^{\gamma k_{22}}$, and collocate ε_{12} at points $\xi^{\gamma k_{12}}$.

By selecting enough collocation equations, the vector $\boldsymbol{\alpha}$ can be expressed in terms of the nodal displacement vector $\mathbf{q}$:

$$\boldsymbol{\alpha} = \mathbf{C}\mathbf{q} \tag{43}$$

Therefore, strain and stress fields are expressed in terms of $\mathbf{q}$, as:

$$\boldsymbol{\varepsilon} = \mathbf{A}(\xi^{\gamma})\mathbf{C}\mathbf{q} = \mathbf{B}^{*}(\xi^{\gamma})\mathbf{q} \tag{44}$$

$$\boldsymbol{\sigma} = \mathbf{D}\mathbf{A}(\xi^{\gamma})\mathbf{C}\mathbf{q} = \mathbf{D}\mathbf{B}^{*}(\xi^{\gamma})\mathbf{q} \tag{45}$$

We substitute (44) and (22) into the principle of minimum potential energy (18):

$$\begin{aligned}
&\delta\pi_5(\mathbf{q}) = 0 \\
&= \delta \sum_m \left\{ \int_{\Omega m} \left[\frac{1}{2}\mathbf{q}^T \mathbf{B}^{*T}(\xi^\gamma)\mathbf{D}\mathbf{B}^*(\xi^\gamma)\mathbf{q} - \mathbf{q}^T \mathbf{N}^T(\xi^\alpha)\bar{\mathbf{f}} \right] d\Omega - \int_{S_{tm}} \mathbf{q}^T \mathbf{N}^T(\xi^\gamma)\bar{\mathbf{t}} dS \right\} \\
&= \sum_m \left[\delta\mathbf{q}^T \int_{\Omega m} \mathbf{B}^{*T}(\xi^\gamma)\mathbf{D}\mathbf{B}^*(\xi^\gamma) d\Omega \mathbf{q} - \delta\mathbf{q}^T \left(\int_{\Omega m} \mathbf{N}^T(\xi^\gamma)\bar{\mathbf{f}} d\Omega + \int_{S_{tm}} \mathbf{N}^T(\xi^\gamma)\bar{\mathbf{t}} dS \right) \right] \\
&= \sum_m \left(\delta\mathbf{q}^T \mathbf{K}^{\mathbf{e}} \mathbf{q} - \delta\mathbf{q}^T \mathbf{Q} \right)
\end{aligned} \tag{46}$$

We notice that such a finite element formulation does not involve any matrix inversion. Because $\boldsymbol{\varepsilon}(\xi^r) = \mathbf{B}^*(\xi^\gamma)\mathbf{q}$ can usually be determined analytically beforehand, the stiffness matrix can be determined analytically, or numerically using very few quadrature points. Moreover, because no Lagrangian multiplier or saddle point problem is involved, this approach is not plagued by LBB conditions. We denote this finite element method as HMFEM2.

In section 4.1, we have illustrated why HMFEM2 is efficient and stable. In section 4.2, we study two other properties which are considered very important for developing any kind of finite elements—ability to pass the patch test and element invariance.

We note that the pioneering concepts of finite-volume mixed approaches, similar to those presented here, in the context of the Meshless Local Petrov-Galerkin method, and without involving the LBB conditions, were presented for solid mechanics problems [Atluri, Han and Rajendran (2004)], and for fluid mechanics problems [Avila, Han and Atluri (2011)].

4.2 On Patch Test and Element Invariance

4.2.1 Patch Test

Patch test requires that any arbitrary linear displacement field can theoretically be exactly reproduced by using a small number of elements in the patch. It is clear that HMFEM1 can pass the constant strain patch test, as long as linear displacement field and constant strain field can be represented by $\mathbf{N}(\xi^r)\mathbf{q}$ and $\mathbf{A}(\xi^r)\boldsymbol{\alpha}$. On the other hand, in the derivation of HMFEM2, we substituted $\boldsymbol{\varepsilon} = \mathbf{A}(\xi^r)\mathbf{C}\mathbf{q} = \mathbf{B}^*(\xi^r)\mathbf{q}$ into the principle of minimum potential energy (18) to formulate finite element equations. Although this relation is reasonably derived by collocation method, the strain and displacement-gradient compatibility (3) is not satisfied everywhere in Ω_m. This is a violation of the requirement of the principle of minimum potential

energy (18), thus it is not guaranteed that arbitrarily developed elements of HMFEM2 can pass the patch test, even if $\mathbf{N}(\xi^r)\mathbf{q}$ and $\mathbf{A}(\xi^r)\boldsymbol{\alpha}$ can represent arbitrary linear displacement field and its corresponding constant strain field. We study the conditions under which HMFEM2 can pass the patch test.

In the constant strain patch test, current formulation of HMFEM2 leads to:

$$\begin{aligned}
&\sum_m \left(\int_{\Omega m} \delta\mathbf{q}^T \mathbf{B}^{*T}(\xi^r)\mathbf{D}\mathbf{B}^*(\xi^r)\mathbf{q}d\Omega - \int_{S_{tm}} \delta\mathbf{q}^T \mathbf{N}^T(\xi^r)\bar{\mathbf{t}}dS \right) \\
&= \sum_m \left(\int_{\Omega m} \delta\mathbf{q}^T \mathbf{B}^T(\xi^r)\mathbf{D}\mathbf{B}^*(\xi^r)\mathbf{q}d\Omega - \int_{S_{tm}} \delta\mathbf{q}^T \mathbf{N}^T(\xi^r)\bar{\mathbf{t}}dS \right) \\
&+ \sum_m \left[\int_{\Omega m} \delta\mathbf{q}^T \left(\mathbf{B}^*(\xi^r) - \mathbf{B}^T(\xi^r)\right)\mathbf{D}\mathbf{B}^*(\xi^r)\mathbf{q}d\Omega \right] \\
&= \sum_m \left\{ \int_{\Omega m} \delta\mathbf{q}^T \mathbf{B}^T(\xi^r)\mathbf{D}\boldsymbol{\varepsilon}_c d\Omega - \int_{S_{tm}} \delta\mathbf{q}^T \mathbf{N}^T(\xi^r)\bar{\mathbf{t}}dS \right\} \\
&+ \sum_m \left[\int_{\Omega m} \delta\mathbf{q}^T \left(\mathbf{B}^*(\xi^r) - \mathbf{B}^T(\xi^r)\right)\mathbf{D}\boldsymbol{\varepsilon}_c d\Omega \right]
\end{aligned} \tag{47}$$

$\boldsymbol{\varepsilon}_c$ indicates the constant strain field of the patch test. It can be seen all the terms vanish in (47) except the last term.

Therefore, in addition to requiring that $\mathbf{N}(\xi^\gamma)\mathbf{q}$ and $\mathbf{B}^*(\xi^\gamma)\mathbf{q}$ can represent arbitrary linear displacement field and its corresponding constant strain field, patch test also requires that the following condition is satisfied:

$$\sum_m \int_{\Omega_m} \mathbf{B}^*(\xi^r)d\Omega\delta\mathbf{q} = \sum_m \int_{\Omega_m} \mathbf{B}(\xi^r)d\Omega\delta\mathbf{q} \;\forall \text{ admissible } \delta\mathbf{q} \tag{48}$$

This is identical to:

$$\sum_m \int_{\Omega_m} \varepsilon_{ij}(\xi^{\gamma k}, \delta\boldsymbol{\alpha})d\Omega = \sum_m \int_{\Omega_m} u_{(i,j)}(\xi^{\gamma k}, \delta\mathbf{q})d\Omega \;\forall \delta\boldsymbol{\alpha} = \mathbf{C}\delta\mathbf{q} \tag{49}$$

where $\varepsilon_{ij}(\xi^{\gamma k}, \delta\boldsymbol{\alpha})$ and $u_{(i,j)}(\xi^{\gamma k}, \delta\mathbf{q})$ are strains derived from $\delta\boldsymbol{\alpha}$ and $\delta\mathbf{q}$ respectively. We have pointed out that violation of strain displacement-gradient compatibility (3) may cause the inability of HMFEM2 to pass the patch test. From (49), we can more clearly see that HMFEM2 can pass the patch test if the strain field derived from $\delta\boldsymbol{\alpha}$ and $\delta\mathbf{q}$ are compatible at least in a finite-volume weak sense. Therefore, when deriving HMFEM2, collocation points should be selected such that (48) or equivalently (49) is satisfied.

We notice that $\int_{\Omega_m} \mathbf{B}(\xi^r)d\Omega = \int_{\Omega_m} \mathbf{B}(\xi^r)\,|\mathbf{J}|d\xi^r$ can be exactly evaluated using numerical quadrature, because $\mathbf{B}(\xi^r)\,|\mathbf{J}|$ are simple polynomials. Therefore, if we

assume $\varepsilon_{ij}(\xi^{\gamma k}, \delta\boldsymbol{\alpha})$ to be simple polynomials, and choose quadrature points as collocations points, (48) and (49) can be made to be exactly satisfied. And thus the developed elements can pass the patch test.

4.2.2 Element Invariance

Invariance is a desired property of every developed finite element, because it is an inherent characteristic of the physical phenomenon, which we try to model with finite elements. Invariance requires that the property of an element, which is an approximation of a patch of real physical object, should not vary according to the observer's point of view. For example, consider a two-dimensional element as illustrated in Fig. 1, if one derives the stiffness matrix in two arbitrary Cartesian coordinates systems $x_1 - x_2$ and $\bar{x}_1 - \bar{x}_2$ respectively, element invariance indicates that:

$$\frac{1}{2}\mathbf{q}^T\mathbf{K}\mathbf{q} = \frac{1}{2}\overline{\mathbf{q}}^T\overline{\mathbf{K}}\overline{\mathbf{q}},\ \forall\overline{\mathbf{q}} = \mathbf{Q}\mathbf{q} \tag{50}$$

where $\mathbf{K}$ and $\overline{\mathbf{K}}$ are stiffness matrices derived in these two different Cartesian coordinate systems, $\mathbf{q}$ and $\overline{\mathbf{q}}$ represent components of element nodal displacements, in base vectors of these two Cartesian coordinate systems $\mathbf{e}_i$ and $\bar{\mathbf{e}}_i$. $\mathbf{Q}$ is the corresponding transfer matrix between $\mathbf{q}$ and $\overline{\mathbf{q}}$.

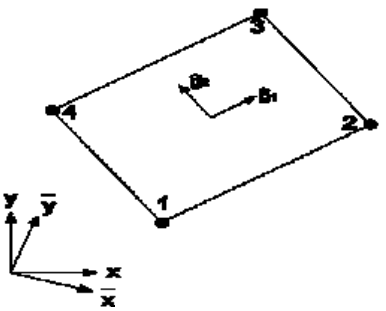

Figure 1: Illustration of invariance of finite elements

[Spilker, Maskeri and Kania (1981), Sze, Chow and Chen (1992)] studied the invariance of hybrid/mixed elements, and concluded that the assumed stress/strain and displacement field should be invariant in order for the derived element to be invariant. For HMFEM1 and HMFEM2, compatibly assumed isoparametric displacement field is obviously invariant. Regarding invariance of the strain field, if strain components in $\mathbf{e}_i, \mathbf{e}_j$ are assumed as $\varepsilon_{ij} = f_{ij}(\xi^{\gamma}, \boldsymbol{\alpha})$, invariance requires

that, for $\varepsilon_{ij} = f_{ij}(\xi^\gamma, \boldsymbol{\alpha})$ with arbitrary $\boldsymbol{\alpha}$, one can always find a $\boldsymbol{\beta}$, such that $\bar{\varepsilon}_{ij} = \varepsilon_{kl}(\mathbf{e}_k \cdot \bar{\mathbf{e}}_i)(\mathbf{e}_l \cdot \bar{\mathbf{e}}_j) = f_{ij}(\xi^\gamma, \boldsymbol{\beta})$, where ε_{ij} and $\bar{\varepsilon}_{ij}$ are components of the strain tensor in $\mathbf{e}_i, \mathbf{e}_j$ and $\bar{\mathbf{e}}_i, \bar{\mathbf{e}}_j$ respectively. On the other hand, one can also assume $\hat{\varepsilon}^{ij} = f^{ij}(\xi^\gamma, \boldsymbol{\alpha})$, where $\hat{\varepsilon}^{ij}$ are the contravariant components of the strain tensor in the element-fixed local base vectors $\hat{\mathbf{g}}_i, \hat{\mathbf{g}}_j$, such that $\varepsilon_{ij} = \hat{\varepsilon}^{kl}(\hat{\mathbf{g}}_k \cdot \mathbf{e}_i)(\hat{\mathbf{g}}_l \cdot \mathbf{e}_j)$. Strain field assumed in this way is always invariant, because the local base vectors $\hat{\mathbf{g}}_i$ do not vary with respect to change of the global coordinate system, as they are element-fixed.

In section 4.3, we consider the plane four-node isoparametric element as an example, to illustrate how to develop elements of HMFEM2. By adopting different strain field assumptions and using different collocation points, two different elements are developed, both of which belong to the family of HMFEM2. Corresponding elements which belong to the family of HMFEM1 are also developed. Their properties regarding efficiency, stability, locking, invariance, and ability to pass the patch test are discussed.

4.3 Some Examples of Four-node Isoparametric Elements

Consider a four-node isoparametric element as seen in Fig. 2. Some points are marked for convenience of illustration, including: center point (which is also the point for a one-point Gauss integration) 0; nodal points 9, 10, 11, 12; edge midpoints 5, 6, 7, 8; 2 by 2 Gaussian integration points 9, 10, 11, 12; 1 by 2 Gaussian integration points 13, 15; 2 by 1 Gaussian integration points 14, 16.

The interpolations of the Cartesian coordinates and the displacement field in the isoparametric element are:

$$x_i = x_i^{(1)} N^{(1)}(\xi^\gamma) + x_i^{(2)} N^{(2)}(\xi^\gamma) + x_i^{(3)} N^{(3)}(\xi^\gamma) + x_i^{(4)} N^{(4)}(\xi^\gamma) \tag{51}$$

$$u_i = u_i^{(1)} N^{(1)}(\xi^\gamma) + u_i^{(2)} N^{(2)}(\xi^\gamma) + u_i^{(3)} N^{(3)}(\xi^\gamma) + u_i^{(4)} N^{(4)}(\xi^\gamma) \tag{52}$$

If one substitutes the displacement field assumption (52) into the principle of minimum potential energy (18), the derived displacement-based primal finite element (DPFEM) is the so-called Q4 element, with $\mathbf{K}^e = \int_{\Omega m} \mathbf{B}^T(\xi^\alpha)\mathbf{D}\mathbf{B}(\xi^\alpha) d\Omega$. We use DPFEM-Q4 to denote such an element. DPFEM-Q4 does not involve LBB conditions, because no Lagrangian multiplier is involved. It is also computationally efficient, if one does not consider that fact that $\int_{\Omega m} \mathbf{B}^T(\xi^\alpha)\mathbf{D}\mathbf{B}(\xi^\alpha) d\Omega$ cannot be exactly evaluated by numerical quadrature. DPFEM-Q4 can also pass the patch test and is invariant. However, it is well-known that DPFEM-Q4 suffers from locking, because the derived strains from assumed displacement field are incomplete and locked together.

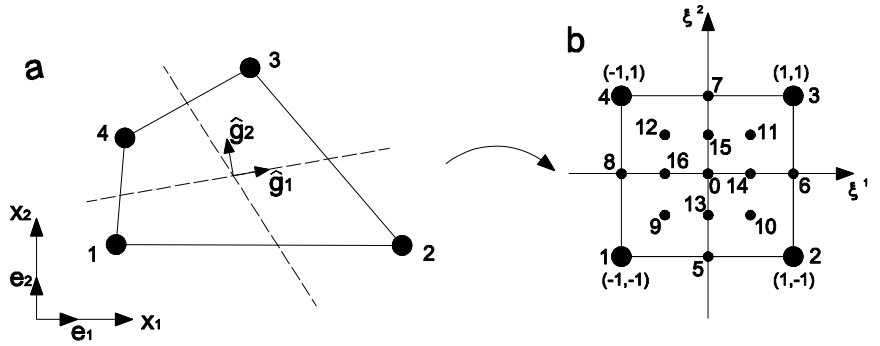

Figure 2: Two-dimensional quadrilateral element: (a) Cartesian coordinates (b) curvilinear (non-dimensional) coordinates

In order to eliminate locking, we can independently assume the contravariant strain components, in the element-fixed curvilinear (non-dimensional) coordinates ξ^r as:

$$\begin{aligned}\hat{\varepsilon}^{11} &= \alpha_1 + \alpha_2 \xi^2 \\ \hat{\varepsilon}^{22} &= \alpha_3 + \alpha_4 \xi^1 \\ \hat{\varepsilon}^{12} &= \alpha_5\end{aligned} \tag{53}$$

such that

$$\varepsilon_{ij} = \hat{\varepsilon}^{kl}(\hat{\mathbf{g}}_k \cdot \mathbf{e}_i)(\hat{\mathbf{g}}_l \cdot \mathbf{e}_j) \tag{54}$$

where $\mathbf{e}_1, \mathbf{e}_2$ are base vectors of the global Cartesian coordinate system, and $\hat{\mathbf{g}}_1, \hat{\mathbf{g}}_2$ are chosen as a set of element-fixed orthonormal local base vectors defined in such a way: $\hat{\mathbf{g}}_1$ is in the same direction of covariant base vector $\mathbf{g}_1$, evaluated at center 0, and $\hat{\mathbf{g}}_2$ is obtained by rotating $\hat{\mathbf{g}}_1$around $\mathbf{e}_3$counterclockwise by 90°, see Fig. 2. From our analysis in section 4.2.2, it is obvious that hybrid/mixed elements derived using strain assumption (53) are invariant, because $\hat{\mathbf{g}}_1, \hat{\mathbf{g}}_2$ are element-fixed, they do not vary with respect to change of the global coordinate system. We also point out that, we choose such a set of element-fixed orthonormal base vectors $\hat{\mathbf{g}}_1, \hat{\mathbf{g}}_2$ instead of using covariant base vectors $\mathbf{g}_1, \mathbf{g}_2$, because $\hat{\mathbf{g}}_1, \hat{\mathbf{g}}_2$ is simply a rotation of $\mathbf{e}_1, \mathbf{e}_2$, while $\mathbf{g}_1, \mathbf{g}_2$ involves distortions of $\mathbf{e}_1, \mathbf{e}_2$. Therefore, assuming strain components in $\hat{\mathbf{g}}_1, \hat{\mathbf{g}}_2$ is expected to result in elements which are less sensitive to mesh distortion, as compared to assuming strain components in $\mathbf{g}_1, \mathbf{g}_2$.

If one substitutes the displacement assumption (52), and the strain field assumption (53) into the two-field variational principle (17), one derives an element stiffness

matrix $\mathbf{K}^e = \mathbf{G}^T\mathbf{H}^{-1}\mathbf{G}$ which belongs to the family of HMFEM1. We denote this element as HMFEM1-a. HMFEM1-a can pass the patch test and is able to avoid locking. However, HMFEM1-a is computationally inefficient, because one needs to evaluate $\mathbf{H}^{-1}$ for each and every element, and evaluate $\mathbf{H}$ and $\mathbf{G}$ over each element. HMFEM1-a also involves the so-called LBB conditions.

On the other hand, if one enforces the compatibility of $\hat{\varepsilon}_{ij}$ and $\hat{u}_{(i,j)}$ at a finite number of collocation points, and substitutes the derived strain field into the principle of minimum potential energy (18), an element which belongs to the family of HMFEM2 will be obtained. However, as shown in section 4.2.1, collocation points should not be arbitrarily selected. For example, if we collocate $\hat{\varepsilon}_{11}$ at point 5, 7, $\hat{\varepsilon}_{22}$ at point 6, 8, and $\hat{\varepsilon}_{12}$ at center 0, the derived element will not be able to pass the patch test. In order to pass the patch test, we should select quadrature points as collocation points.

For simplicity of further illustration, we decompose the corresponding matrix $\mathbf{B}(\xi^\gamma)$ as in (23) into $\mathbf{B}_{11}(\xi^\gamma), \mathbf{B}_{22}(\xi^\gamma), \mathbf{B}_{12}(\xi^\gamma)$, which are the rows corresponding to $u_{(1,1)}, u_{(2,2)}, u_{(1,2)}$ respectively. We further denote the value of $\mathbf{B}_{ij}(\xi^\gamma)$ at point k as $\mathbf{B}_{ij}^k$. For example, $u_{(1,2)}(\xi^1 = \xi^2 = 0) = \mathbf{B}_{12}^0\mathbf{q}$. Similarly, we decompose the corresponding $\hat{\mathbf{B}}(\xi^\gamma)$ into $\hat{\mathbf{B}}_{11}(\xi^\gamma), \hat{\mathbf{B}}_{22}(\xi^\gamma), \hat{\mathbf{B}}_{12}(\xi^\gamma)$, and denote the value of $\hat{\mathbf{B}}_{ij}(\xi^\gamma)$ at point k as $\hat{\mathbf{B}}_{ij}^k$.

By collocating $\hat{\varepsilon}_{11}$ at point 13, 15, $\hat{\varepsilon}_{22}$ at point 14, 16, and $\hat{\varepsilon}_{12}$ at center 0, the following strain field is obtained:

$$\begin{aligned}
\hat{\varepsilon}_{11} &= \frac{1}{2}\left(\hat{\mathbf{B}}_{11}^{13}\mathbf{q} + \hat{\mathbf{B}}_{11}^{15}\mathbf{q}\right) + \frac{\sqrt{3}}{2}\xi^2\left(-\hat{\mathbf{B}}_{11}^{13}\mathbf{q} + \mathbf{B}_{11}^{15}\hat{\mathbf{q}}\right) \\
\hat{\varepsilon}_{22} &= \frac{1}{2}\left(\hat{\mathbf{B}}_{22}^{14}\mathbf{q} + \hat{\mathbf{B}}_{22}^{16}\mathbf{q}\right) + \frac{\sqrt{3}}{2}\xi^1\left(\hat{\mathbf{B}}_{22}^{14}\mathbf{q} - \hat{\mathbf{B}}_{22}^{16}\mathbf{q}\right) \\
\hat{\varepsilon}_{12} &= \hat{\mathbf{B}}_{12}^0\mathbf{q} \\
\text{and } \varepsilon_{ij} &= \hat{\varepsilon}^{kl}(\hat{\mathbf{g}}_k \cdot \mathbf{e}_i)(\hat{\mathbf{g}}_l \cdot \mathbf{e}_j)
\end{aligned} \tag{55}$$

We rewrite (55) as $\boldsymbol{\varepsilon} = \mathbf{B}^*(\xi^r)\mathbf{q}$ and substituting it into the principle of minimum potential energy (18), an element which belongs to the family of HMFEM2 is obtained. We denote this element as HMFEM2-a. The stiffness matrix of HMFEM2-a is $\mathbf{K}^e = \int_{\Omega m}\mathbf{B}^{*T}(\xi^r)\mathbf{D}\mathbf{B}^*(\xi^r)d\Omega$. HMFEM2-a is locking-free, invariant, and able to pass the patch test. In addition, HMFEM2-a does not involve LBB conditions, and it is stable because the stiffness matrix can be easily shown to be rank-sufficient. However, HMFEM2-a is still not as computationally efficient as DPFEM-Q4, because additional computational burden is required to calculate the B matrix at each collocation point.

To make the computation more efficient, and to make the strain field assumption

more complete, one can further assume the strain field as (we do not correspondingly assume $\varepsilon_{12} = \gamma_1 + \gamma_2\xi^1 + \gamma_3\xi^2 + \gamma_4\xi^1\xi^2$ in order to avoid locking):

$$\begin{aligned}
\varepsilon_{11} &= \alpha_1 + \alpha_2\xi^1 + \alpha_3\xi^2 + \alpha_4\xi^1\xi^2 \\
\varepsilon_{22} &= \beta_1 + \beta_2\xi^1 + \beta_3\xi^2 + \beta_4\xi^1\xi^2 \\
\varepsilon_{12} &= \gamma_1
\end{aligned} \tag{56}$$

From our analysis in section 4.2.2, we can see that hybrid/mixed elements derived using strain field assumption (56) are also invariant.

If one substitutes the displacement assumptions (52), and the strain field assumption (56) into the two-field variational principle (17), following the same procedure of deriving HMFEM1-a, one derives an element which belongs to the family of HMFEM1, denoted as HMFEM1-b. However, HMFEM1-b is computationally inefficient, because one needs to evaluate $\mathbf{H}^{-1}$, which is a 9 by 9 matrix, for each and every element.

On the other hand, following a similar procedure of developing HMFEM2-a, one can derive another element which belongs to the family of HMFEM2. Similarly to HMFEM2-a, one should not select arbitrary collocation points. For example, if we collocate $\varepsilon_{11}, \varepsilon_{22}$ at nodal points 1, 2, 3, 4, and collocate ε_{12} at center point 0, the derived element cannot pass the patch test. Instead, we should select quadrature points as collocation points. By collocating $\varepsilon_{11}, \varepsilon_{22}$ at Gaussian integration points 1, 2, 3, 4, and collocating ε_{12} at center point 0, the following strain field is obtained:

$$\begin{aligned}
\varepsilon_{11} &= N^{(1)}(\sqrt{3}\xi^r)\mathbf{B}_{11}^{9}\mathbf{q} + N^{(2)}(\sqrt{3}\xi^r)\mathbf{B}_{11}^{10}\mathbf{q} + N^{(3)}(\sqrt{3}\xi^r)\mathbf{B}_{11}^{11}\mathbf{q} + N^{(4)}(\sqrt{3}\xi^r)\mathbf{B}_{11}^{12}\mathbf{q} \\
\varepsilon_{22} &= N^{(1)}(\sqrt{3}\xi^r)\mathbf{B}_{22}^{9}\mathbf{q} + N^{(2)}(\xi^r)\mathbf{B}_{22}^{10}\mathbf{q} + N^{(3)}(\sqrt{3}\xi^r)\mathbf{B}_{22}^{11}\mathbf{q} + N^{(4)}(\sqrt{3}\xi^r)\mathbf{B}_{22}^{12}\mathbf{q} \\
\varepsilon_{12} &= \mathbf{B}_{12}^{0}\mathbf{q}
\end{aligned} \tag{57}$$

We denote the element derived in this way as HMFEM2-b. HMFEM2-b is stable, locking-free, invariant, and is able to pass the patch test. Moreover, we notice that, in order to evaluate the stiffness matrix of HMFEM2-b, exactly only 2 by 2 Gaussian integration points are needed. Therefore, one does not even need to derive (57). One can just follow the same procedure of evaluating stiffness matrix of DPFEM1-Q4, using 2 by 2 Gaussian integration points, by only substituting $\mathbf{B}_{12}(\xi^r)$ with $\mathbf{B}_{12}^{0}$ at every Gaussian point. Derived in this way, the computational burden of HMFEM2-b is even less than DPFEM-Q4, in the sense that the stiffness matrix of DPFEM-Q4 cannot be evaluated exactly using even a large number of quadrature points, because rational functions are involved in the integrand of $\int_{\Omega m}\mathbf{B}^T(\xi^\alpha)\mathbf{D}\mathbf{B}(\xi^\alpha)d\Omega$.

From our analysis, we consider HMFEM2-b to be highly useful, because it is efficient, stable, locking-free, invariant and able to pass the patch test, with only trivial changes to the famous DPFEM-Q4 element. We also point out that the essential idea of HMFEM2 can be extended to elements of higher-order, higher-dimension, and for other physical problems. In section 5, we extend this idea to Voronoi cell finite element method, for micromechanical analysis of materials.

5 Extension to Voronoi Cell Finite Element Method

[Ghosh and Mallett (1994); Ghosh, Lee and Moorthy (1995)] proposed the idea of discretizing the solution domain using Dirichlet tessellation, and developing corresponding Voronoi cell finite elements (VCFEM)/polygonal finite elements to solve problems of micromechanics of materials. However, the underlying theoretical foundation of the VCFEM proposed by [Ghosh and his co-workers (1994, 1995 and many more in the past 20 years)] is the modified principle of minimum complementary energy (16), based on "a priori equilibrated" stress field inside each element, and continuous displacement along element edges. Similar to the hybrid stress elements in [Pian (1964)], three major drawbacks of such a VCFEM can be readily seen: selection of "a priori equilibrated" stress field is difficult or even impossible for geometrically nonlinear (finite deformation) and dynamical problems; matrix inversion, involved in developing the stiffness matrix of each and every element, makes such a VCFEM computationally inefficient; Lagrangian multipliers involved in such a two-field variational principle make the derived elements suffer from LBB conditions, which are almost impossible to be satisfied a priori.

In this section, we derive a new and much simpler type of VCFEM in two-dimensional problems, in order to avoid the aforementioned drawbacks. For an arbitrary polygonal element as in Fig. 3 with n nodes $\mathbf{x}^1, \mathbf{x}^2, ..., \mathbf{x}^n$, with corresponding nodal displacements $u_i^1, u_i^2, ..., u_i^n$, a linear displacement field assumption along each edge is used:

$$u_i^E = \sum_{k=1}^{n} N^k(\mathbf{x}) u_i^k \text{ at } \partial\Omega_m \tag{58}$$

On the other hand, a displacement field inside each element is assumed as compactly supported radial basis functions (CS-RBF). CS-RBF have been suggested and widely used recently, see [Wu (1995); Atluri, Han and Rajendran (2004)]. The reasons why we choose CS-RBF as our interior displacement field assumption are their Dirac delta property, positive-definiteness, and relatively simple forms of spatial derivatives. Moreover, the lack of their completeness has been overcome by introducing additional polynomial functions as in [Golberg, Chen and Bowman

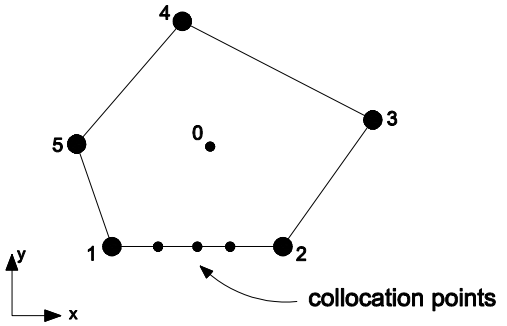

Figure 3: A two-dimensional polygonal element

(1999)]. Under such an assumption, the interior displacement field is represented as:

$$u_i^I = \mathbf{R}^{\mathbf{T}}(\mathbf{x})\mathbf{a} + \mathbf{P}^{\mathbf{T}}(\mathbf{x})\mathbf{b} \text{ in } \Omega_m \tag{59}$$

where $\mathbf{R}^{\mathbf{T}}(\mathbf{x}) = \begin{bmatrix} R^{r1}(\mathbf{x}) & R^{r2}(\mathbf{x}) & \dots & R^{rl}(\mathbf{x}) \end{bmatrix}$ is a set of radial basis functions centered at l points $\mathbf{x}^{r1}, \mathbf{x}^{r2} \dots \mathbf{x}^{rl}$ along $\partial\Omega_m$; $\mathbf{P}^{\mathbf{T}}(\mathbf{x}) = \begin{bmatrix} P^1(\mathbf{x}) & P^2(\mathbf{x}) & \dots & P^m(\mathbf{x}) \end{bmatrix}$ is set of monomial functions which is complete to a certain order; $\mathbf{a}, \mathbf{b}$ are coefficient vectors.

While various radial basis functions can be used, in the current study, we use:

$$R^{rl}(\mathbf{x}) = \begin{cases} \left(1 - \frac{d^{rl}(\mathbf{x})}{r^{rl}}\right)^3 \left(1 + 3\frac{d^{rl}(\mathbf{x})}{r^{rl}}\right) & d^{rl}(\mathbf{x}) < r^{rl} \\ 0 & d^{rl}(\mathbf{x}) \geq r^{rl} \end{cases} \tag{60}$$

where $d^{rl}(\mathbf{x}) = \left|\mathbf{x} - \mathbf{x}^{rl}\right|$ is the Euclidean distance from point $\mathbf{x}$to point $\mathbf{x}^{rl}$, r^{rl} is the support size of $R^{rl}(\mathbf{x})$.

And we use first-order complete polynomial basis:

$$\mathbf{P}^{\mathbf{T}}(\mathbf{x}) = \begin{bmatrix} 1 & x & y \end{bmatrix} \tag{61}$$

The coefficients are obtained by enforcing the compatibility condition of the interior and the edge displacements at collocation points $\mathbf{x}^{r1}, \mathbf{x}^{r2} \dots \mathbf{x}^{rl}$, which leads to:

$$\begin{bmatrix} \mathbf{R}_0 & \mathbf{P}_0 \\ \mathbf{P}_0^T & \mathbf{0} \end{bmatrix} \begin{Bmatrix} \mathbf{a} \\ \mathbf{b} \end{Bmatrix} = \begin{Bmatrix} \mathbf{u}_i^r \\ \mathbf{0} \end{Bmatrix} \tag{62}$$

where

$$\mathbf{R_0} = \begin{bmatrix} R^{r1}(\mathbf{x}^{r1}) & R^{r2}(\mathbf{x}^{r1}) & \dots & R^{rl}(\mathbf{x}^{r1}) \\ R^{r1}(\mathbf{x}^{r2}) & R^{r2}(\mathbf{x}^{r2}) & \dots & R^{rl}(\mathbf{x}^{r2}) \\ \vdots & \vdots & \ddots & \vdots \\ R^{r1}(\mathbf{x}^{rl}) & R^{r2}(\mathbf{x}^{rl}) & \dots & R^{rl}(\mathbf{x}^{rl}) \end{bmatrix} \tag{63}$$

$$\mathbf{P_0} = \begin{bmatrix} P^{1}(\mathbf{x}^{r1}) & P^{2}(\mathbf{x}^{r1}) & \dots & P^{m}(\mathbf{x}^{r1}) \\ P^{1}(\mathbf{x}^{r2}) & P^{2}(\mathbf{x}^{r2}) & \dots & P^{m}(\mathbf{x}^{r2}) \\ \vdots & \vdots & \ddots & \vdots \\ P^{1}(\mathbf{x}^{rl}) & P^{2}(\mathbf{x}^{rl}) & \dots & P^{m}(\mathbf{x}^{rl}) \end{bmatrix} \tag{64}$$

$$\begin{aligned} \mathbf{u}_i^{rT} &= \begin{bmatrix} u_i^{r1} & u_i^{r2} & \cdots & u_i^{rl} \end{bmatrix} \\ &= \begin{bmatrix} \sum_{k=1}^{n} N^k(\mathbf{x}^{r1}) u_i^k & \sum_{k=1}^{n} N^k(\mathbf{x}^{r2}) u_i^k & \cdots & \sum_{k=1}^{n} N^k(\mathbf{x}^{rl}) u_i^k \end{bmatrix} \end{aligned} \tag{65}$$

By solving (62), the interior displacement field is interpolated as:

$$u_i^I = \left[\mathbf{R^T}(\mathbf{x})\mathbf{G}_r + \mathbf{P^T}(\mathbf{x})\mathbf{G}_p\right]\mathbf{u}_i^r = \sum_{k=1}^{n} N^{*k}(\mathbf{x}) u_i^k \tag{66}$$

Summarizing (58)-(66), edge and interior displacement field are all expressed in terms of nodal displacement vector $\mathbf{q}$:

$$\mathbf{u}^E = \mathbf{N}(\mathbf{x})\mathbf{q} \text{ at } \partial\Omega_m \tag{67}$$

$$\mathbf{u}^I = \mathbf{N}^*(\mathbf{x})\mathbf{q} \text{ in } \Omega_m \tag{68}$$

And the corresponding interior strains are:

$$\mathbf{u}^I_{(i,j)} = \mathbf{B}^*(\mathbf{x})\mathbf{q} \text{ in } \Omega_m \tag{69}$$

Using the principle of minimum potential energy (18), we obtain the finite element equations:

$$\begin{aligned} &\delta\pi_5(\mathbf{q}) = 0 \\ &= \delta \sum_m \left\{ \int_{\Omega m} \left[\frac{1}{2}\mathbf{q}^T \mathbf{B}^{*T}(\mathbf{x}) \mathbf{D} \mathbf{B}^*(\mathbf{x})\mathbf{q} - \mathbf{q}^T \mathbf{N}^{*T}(\mathbf{x})\bar{\mathbf{f}} \right] d\Omega - \int_{S_{tm}} \mathbf{q}^T \mathbf{N}^T(\mathbf{x})\bar{\mathbf{t}} dS \right\} \end{aligned}$$

$$\sum_m \left[\delta \mathbf{q}^T \int_{\Omega m} \mathbf{B}^{*T}(\mathbf{x}) \mathbf{D} \mathbf{B}^*(\mathbf{x}) d\Omega \mathbf{q} - \delta \mathbf{q}^T \left(\int_{\Omega m} \mathbf{N}^{*T}(\mathbf{x}) \bar{\mathbf{f}} d\Omega + \int_{S_{tm}} \mathbf{N}^T(\mathbf{x}) \bar{\mathbf{t}} dS \right) \right]$$
$$= \sum_m \left(\delta \mathbf{q}^T \mathbf{K}^{\mathbf{e}} \mathbf{q} - \delta \mathbf{q}^T \mathbf{Q} \right) \tag{70}$$

We denote this novel VCFEM as VCFEM-RBF1.

However, similar to our previous analysis in section 4.2.2, there is no guarantee that VCFEM-RBF1 can pass the constant strain patch test, even though the displacement field trial solutions (67)(68) are first-order complete. This is because displacement field in Ω_m and along $\partial\Omega_m$ are merely made compatible on selected RBF center/collocation points $\mathbf{x}^{r1}, \mathbf{x}^{r2} \ldots \mathbf{x}^{rl}$, which is a violation of the requirement of the principle of minimum potential energy (18). Following the same procedure used in section 4.2.2, we can find the condition to pass the patch test is:

$$\sum_m \int_{\partial\Omega_m} \left[u_i^E(\mathbf{x}, \delta\mathbf{q}) n_j + u_j^E(\mathbf{x}, \delta\mathbf{q}) n_i \right] dS = \sum_m \int_{\partial\Omega_m} \left[u_i^I(\mathbf{x}, \delta\mathbf{q}) n_j + u_j^I(\mathbf{x}, \delta\mathbf{q}) n_i \right] dS \tag{71}$$

where $u_i^E(\mathbf{x}, \delta\mathbf{q})$ and $u_i^I(\mathbf{x}, \delta\mathbf{q})$ are the edge and interior displacements derived from $\delta\mathbf{q}$ respectively. Condition (71) states that the boundary and interior displacement derived from $\delta\mathbf{q}$ should be compatible at least in a finite volume sense. Therefore, it seems reasonable to collocate at the quadrature points along each edge. Moreover, by increasing the number of RBF center/collocation points, the residual error of (71) can be reduced, so that the error produced in patch test will be reduced to a satisfactory level.

Furthermore, VCFEM-RBF1 may suffer from locking because the assumed interior displacement field (68) is only complete to the first order, and the derived strains are locked together. To improve the performance of VCFEM-RBF1, we can further independently assume an interior strain field $\varepsilon_{ij}(\mathbf{x}, \boldsymbol{\alpha})$, which eliminates the shear locking terms, and determine $\boldsymbol{\alpha}$ by enforcing the compatibility between $\varepsilon_{ij}(\mathbf{x}, \boldsymbol{\alpha})$ and $u^I_{(i,j)}(\mathbf{x}, \mathbf{q})$ at several preselected collocation points, following the same procedure of developing HMFEM2.

Similar to what was done in section 4.3, we decompose the corresponding $\mathbf{B}^*(\xi^\gamma)$ as in (70) into $\mathbf{B}^*_{11}(\xi^\gamma), \mathbf{B}^*_{22}(\xi^\gamma), \mathbf{B}^*_{12}(\xi^\gamma)$, which are the rows corresponding to $u^I_{(1,1)}, u^I_{(2,2)}, u^I_{(1,2)}$ respectively. We see that shear strain $\mathbf{B}^*_{12}(\xi^\gamma)\mathbf{q}$ is locked with $\mathbf{B}^*_{11}(\xi^\gamma)\mathbf{q}, \mathbf{B}^*_{22}(\xi^\gamma)\mathbf{q}$ because of the part of strain derived from radial basis function $\mathbf{R}^{\mathbf{T}}(\mathbf{x})$, not the part of strain derived from linear polynomial basis function $\mathbf{P}^{\mathbf{T}}(\mathbf{x})$.

Therefore, we simply use the following strain field assumption, eliminating the part of ε_{12} derived from radial basis function $\mathbf{R^T}(\mathbf{x})$:

$$\begin{aligned}
\varepsilon_{11} &= \mathbf{B}^*_{11}(\mathbf{x})\boldsymbol{\alpha}_{11} \\
\varepsilon_{22} &= \mathbf{B}^*_{22}(\mathbf{x})\boldsymbol{\alpha}_{22} \\
\varepsilon_{12} &= \alpha_{12}
\end{aligned} \tag{72}$$

We collocate $\varepsilon_{11}, \varepsilon_{12}$ at enough points inside Ω_m, and collocate ε_{12} at the center of polygon. This leads to:

$$\begin{aligned}
\varepsilon_{11} &= \mathbf{B}^*_{11}(\mathbf{x})\mathbf{q} \\
\varepsilon_{22} &= \mathbf{B}^*_{22}(\mathbf{x})\mathbf{q} \\
\varepsilon_{12} &= \mathbf{B}^{0*}_{12}\mathbf{q}
\end{aligned} \tag{73}$$

where $\mathbf{B}^{0*}_{12}$ is the value of $\mathbf{B}^*_{12}(\mathbf{x})$ evaluated at the center of the polygon. We rewrite this as:

$$\boldsymbol{\varepsilon} = \mathbf{B}^{**}(\mathbf{x})\mathbf{q} \tag{74}$$

Substituting strain field (74), interior displacement field (68) and edge displacement field (67) into principle of minimum potential energy (18), we obtain the finite element equations:

$$\begin{aligned}
&\delta\pi_5(\mathbf{q}) = 0 \\
&= \delta\sum_m \left\{ \int_{\Omega m} \left[\frac{1}{2}\mathbf{q}^T\mathbf{B}^{**T}(\mathbf{x})\mathbf{D}\mathbf{B}^{**}(\mathbf{x})\mathbf{q} - \mathbf{q}^T\mathbf{N}^{*T}(\mathbf{x})\bar{\mathbf{f}} \right] d\Omega - \int_{S_{tm}} \mathbf{q}^T\mathbf{N}^T(\mathbf{x})\bar{\mathbf{t}}dS \right\} \\
&\sum_m \left[\delta\mathbf{q}^T \int_{\Omega m} \mathbf{B}^{**T}(\mathbf{x})\mathbf{D}\mathbf{B}^{**}(\mathbf{x})d\Omega\mathbf{q} - \delta\mathbf{q}^T \left(\int_{\Omega m} \mathbf{N}^{*T}(\mathbf{x})\bar{\mathbf{f}}d\Omega + \int_{S_{tm}} \mathbf{N}^T(\mathbf{x})\bar{\mathbf{t}}dS \right) \right] \\
&= \sum_m \left(\delta\mathbf{q}^T\mathbf{K}^{\mathbf{e}}\mathbf{q} - \delta\mathbf{q}^T\mathbf{Q} \right)
\end{aligned} \tag{75}$$

We denote this method as VCFEM-RBF2. Similar to our analysis in section 4.3 for the relation between HMFEM2-b and DPFEM-Q4, we can see that the stiffness matrix of VCFEM-RBF2 can be derived using the same procedure of deriving VCFEM-RBF1, only by substituting $\mathbf{B}^*_{12}(\mathbf{x})$ with $\mathbf{B}^{0*}_{12}$ at every quadrature point.

On the other hand, in the VCFEM proposed by [Ghosh and Mallett (1994); Ghosh, Lee and Moorthy (1995)], "a prior equilibrated" stress field is assumed as:

$$\boldsymbol{\sigma} = \mathbf{S}(\mathbf{x})\boldsymbol{\alpha} \text{ in } \Omega_m \tag{76}$$

By substituting stress field (76) and displacement field (67) into the modified principle of minimum complementary energy (16), one obtains:

$$\begin{aligned}
&\delta\pi_3(\boldsymbol{\alpha},\mathbf{q}) = 0 \\
&= \delta\sum_m \left(\frac{1}{2}\boldsymbol{\alpha}^T\mathbf{H}\boldsymbol{\alpha} - \mathbf{q}^T\mathbf{G}^T\boldsymbol{\alpha} + \mathbf{q}^T\mathbf{Q}\right) \\
&= \sum_m \left(\delta\boldsymbol{\alpha}^T\mathbf{H}\boldsymbol{\alpha} - \delta\mathbf{q}^T\mathbf{G}^T\boldsymbol{\alpha} - \delta\boldsymbol{\alpha}^T\mathbf{G}\mathbf{q} + \delta\mathbf{q}^T\mathbf{Q}\right)
\end{aligned} \tag{77}$$

$$\mathbf{G} = \int_{\partial\Omega m} \mathbf{S}^T(\mathbf{x})^T\mathbf{n}^T\mathbf{N}(\mathbf{x})dS \tag{78}$$

$$\mathbf{H} = \int_{\Omega m} \mathbf{S}^T(\mathbf{x})\mathbf{D}^{-1}\mathbf{S}(\mathbf{x})d\Omega \tag{79}$$

$$\mathbf{Q} = \int_{Stm} \mathbf{N}^T(\mathbf{x})\bar{\mathbf{t}}dS \tag{80}$$

which leads to the finite element equations:

$$\sum_m \left(\delta\mathbf{q}^T\mathbf{K}^{\mathbf{e}}\mathbf{q} - \delta\mathbf{q}^T\mathbf{Q}\right) = \sum_m \left(\delta\mathbf{q}^T\mathbf{G}^T\mathbf{H}^{-1}\mathbf{G}\mathbf{q} - \delta\mathbf{q}^T\mathbf{Q}\right) = 0 \tag{81}$$

We denote elements derived in this way as VCFEM-HS (hybrid stress).

Compared to VCFEM-HS, VCFEM-RBF2 has several important advantages:

Firstly, in the development of stiffness matrix of VCFEM-HS, one has to evaluate $\mathbf{H}$ and $\mathbf{G}$ using numerical quadrature (which are high dimensional matrices for polygons with a large number of edges), and carry out the matrix inversion of $\mathbf{H}$. Although VCFEM-RBF2 also involves matrix inversion, it is only in the phase of defining trial solution. Stiffness matrix is directly derived using the principle of minimum potential energy. Therefore, VCFEM-RBF2 is expected to be computationally more efficient than VCFEM-HS.

Secondly, VCFEM-RBF2 is obviously locking-free, because the shear locking terms are eliminated in the independently assumed strain field. On the other hand, independent assumption of stress field is not so straight-forward in the sense of avoiding locking, compared to independent assumption of strain field. Careful attention should be paid to the question of how to assume independent stress field so that the developed elements are not locked.

Thirdly, VCFEM-RBF1,2 are both invariant, because of the assumed displacement and strain field, which has the same formulation irrespective of the number of element edges, is obviously invariant. However, one should carefully pick different invariant stress field assumptions for VCFEM-HS elements with different number of edges, in order for the derived element to be invariant.

Moreover, VCFEM-HS requires selection of "a priori equilibrated" stress field. This is difficult for nonlinear (finite deformation) and dynamical problems, thus limiting most applications of VCFEM-HS to infinitesimal deformation, linear static problems. On the other hand, extension to geometrical nonlinear and dynamical problems for VCFEM-RBF2 is straight-forward.

Finally, because the modified principle of minimum complementary energy (16) involves Lagrangian multipliers, VCFEM-HS suffers from LBB conditions, which are almost impossible to be satisfied a priori, especially for elements with a large number of edges. On the contrary, VCFEM-RBF2 does not involve LBB conditions, because no Lagrangian multipliers are involved in the principle of minimum potential energy (18).

As a summary, we point out that selection of "a priori equilibrated", independent and invariant stress field, which satisfies LBB conditions a priori for VCFEM-HS, is especially difficult for elements with a large number of edges, and impossible for geometrical nonlinear and dynamical problems. On the other hand, VCFEM-RBF2 avoids all of these disadvantages, and is computationally more efficient. Therefore, we recommend VCFEM-RBF2 for engineering applications.

We also point that, there are many other possible ways of developing VCFEMs. In this study, interior displacements are assumed as RBFs. However, there are other kinds of promising displacement field assumptions, such as linear combinations of T-complete functions, as in the T-Trefftz method, and linear combinations of fundamental solutions, as in the F-Trefftz method (or the Method of Fundamental Solution), etc. Moreover, in the present study, collocation method is used to enforce the compatibility of edge and interior displacements in a strong form, at a finite number of collocation points. One can also enforce such a compatibility condition in a weak sense, using the least-square method. All these alternatives seem promising, but they will be reserved for future study, following the same essential idea presented in this study.

6 Numerical Examples

Two-dimensional linear static problems are chosen here to illustrate the performance of different elements. The main properties that are evaluated include: efficiency, stability, invariance, locking, sensitivity to mesh distortion, and convergence rates. The experiments are organized as follows.

In section 6.1, by comparing the eigenvalues of a four-node element derived in the original and rotated coordinate system, the stability and invariance of DPFEM-Q4, HMFEM1-a,b HMFEM2-a,b are evaluated. The CPU time for computing each of these elements are also compared in order to show the computational burden for

each element. In section 6.2, we conduct the so-called constant strain patch test using these elements. In section 6.3, by modeling a cantilever beam under end shear load or bending moment, performances of these elements are evaluated in three aspects: locking, sensitivity to distortion, and convergence rates. In section 6.4, we present numerical experiments specifically designed for VCFEMs.

6.1 Test of Invariance, Stability and Efficiency

Plane stress problems with $E = 1$ and $v = 0.25$ are considered. A square element with four nodes with global Cartesian coordinates $(-1,-1),(1,-1),(1,1),(-1,1)$ is considered. To illustrate our analysis in section 4.2.2 and 4.3, all elements of DPFEM, HMFEM1-a,b and HMFEM2-a,b are firstly derived in the global Cartesian coordinate system. Their eigenvalues are shown in Tab. 1. And the CPU time used for computing each of these elements using 2 by 2 Gaussian integration is shown in Tab. 3, normalized to that for DPFEM-Q4. Then the global Cartesian coordinate system is rotated counterclockwise by 45°. The element stiffness matrices are computed again in this new coordinate system. Their eigenvalue are shown in Tab. 2.

Firstly, we can see that all elements are stable, because only 3 zero eigenvalues exist for each element, which is equal to the number of rigid-body modes. Secondly, by comparing Tab. 1 and Tab. 2, we can clearly see that DPFEM-Q4, HMFEM1-a,b and HMFEM2-a,b are all invariant, because their eigenvalues do not change with respect to the rotation of the global coordinate system. This is consistent with our previous analysis. Finally, from Tab. 3, we can see that HMFEM2-b is the most computationally efficient among these four hybrid/mixed elements. HMFEM1-a,b are computationally inefficient because matrix inversion is involved. HMFEM2-a is also not so efficient as HMFEM2-b, because additional computational burden is required to calculate the B matrix at each collocation point. The computational burden of HMFEM2-b is almost equal to that for DPFEM-Q4, evaluated using 2 by 2 Gauss integration. However, the stiffness matrix of a distorted DPFEM-Q4 element cannot be exactly evaluated by Gauss integration, even though mostly only 2 by 2 Gauss quadrature is used in engineering applications. In this sense, HMFEM2-b is even more efficient than DPFEM-Q4, since the integration is exact for HMFEM2-b.

6.2 Patch Test

This example is a standard patch test, shown in Fig. 4. Plane stress case is considered. The material parameters are taken as $E = 1.0$ and $v = 0.25$. Two mesh configurations are used for the testing purpose: one is regular, and the other is irregular, as shown in Fig. 4. In the patch test, a uniform tensile force is applied

Table 1: Eigenvalues of elements derived in the original coordinate system

Eigenvalues	Elements				
Rotation=0°	DPFEM-Q4	HMFEM1-a	HMFEM1-b	HMFEM2-a	HMFEM2-b
1	1.3333	1.3333	1.3333	1.3333	1.3333
2	0.8000	0.8000	0.8000	0.8000	0.8000
3	0.8000	0.8000	0.8000	0.8000	0.8000
4	0.4889	0.3556	0.3556	0.3556	0.3556
5	0.4889	0.3556	0.3556	0.3556	0.3556
6	0.0000	0.0000	0.0000	0.0000	0.0000
7	0.0000	0.0000	0.0000	0.0000	0.0000
8	0.0000	0.0000	0.0000	0.0000	0.0000

Table 2: Eigenvalues of elements derived in the coordinate system rotated by 45°

Eigenvalues	Elements				
Rotation=45°	DPFEM-Q4	HMFEM1-a	HMFEM1-b	HMFEM2-a	HMFEM2-b
1	1.3333	1.3333	1.3333	1.3333	1.3333
2	0.8000	0.8000	0.8000	0.8000	0.8000
3	0.8000	0.8000	0.8000	0.8000	0.8000
4	0.4889	0.3556	0.3556	0.3556	0.3556
5	0.4889	0.3556	0.3556	0.3556	0.3556
6	0.0000	0.0000	0.0000	0.0000	0.0000
7	0.0000	0.0000	0.0000	0.0000	0.0000
8	0.0000	0.0000	0.0000	0.0000	0.0000

Table 3: CPU time required for computing the stiffness matrix of each element, normalized to that for DPFEM-Q4 element.

CPU	Elements				
Time	DPFEM-Q4	HMFEM1-a	HMFEM1-b	HMFEM2-a	HMFEM2-b
	1.00	1.83	1.78	1.77	1.09

to the upper edge, and proper displacement boundary conditions are applied to the lower edge. The error is defined as follows:

$$Error = \frac{\|\mathbf{q} - \mathbf{q}^{exact}\|}{\|\mathbf{q}^{exact}\|} \tag{82}$$

where $\mathbf{q}$ and $\mathbf{q}^{exact}$ are the computed and exact nodal displacement vector. And $\|\|$ represents the 2-norm.

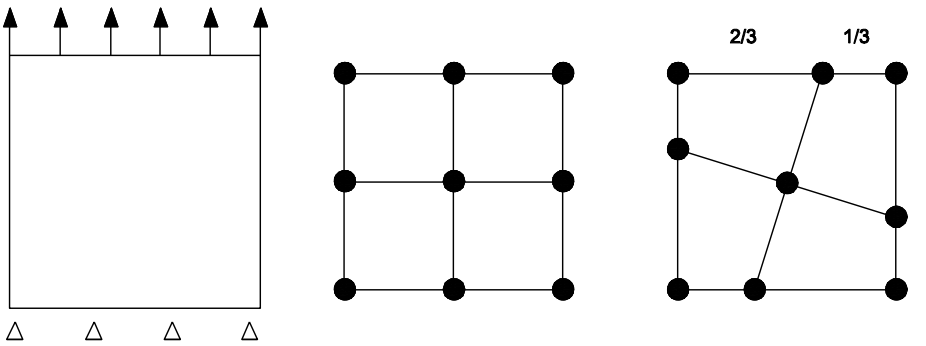

Figure 4: A cube under uniform tension with two mesh configurations

DPFEM-Q4, HMFEM1-a,b and HMFEM2-a,b are used for the patch test, and results are shown in Tab. 4. As expected, all these elements can pass the patch test, and the produced errors are every limited. These results are consistent with our previous analysis in section 4.2.1.

Table 4: Performances of different elements in the constant strain patch test

Mesh	DPFEM-Q4	HMFEM1-a	HMFEM1-b	HMFEM2-a	HMFEM2-b
Regaular	1.2×10^{-15}	7.5×10^{-16}	7.8×10^{-16}	1.1×10^{-15}	1.0×10^{-15}
Irregular	1.2×10^{-15}	5.4×10^{-16}	8.1×10^{-16}	8.1×10^{-16}	9.7×10^{-16}

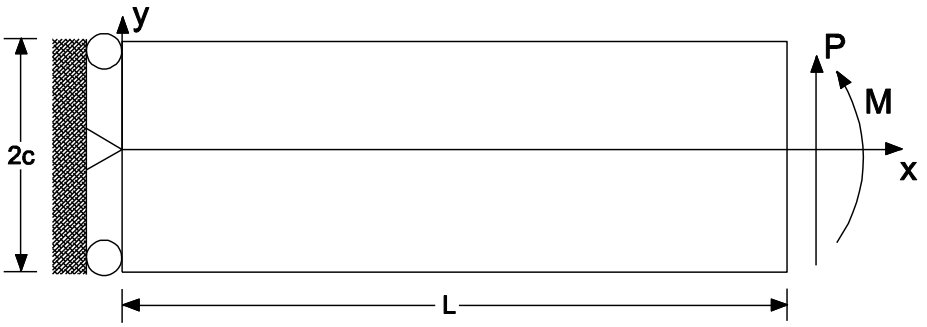

Figure 5: A cantilever beam under an end shear load or bending moment

6.3 Cantilever Beam Test

The performances of different elements are also evaluated, using the problem of a cantilever beam under an end shear load or bending moment. As shown in Fig. 5, the length and height of the beam is L and $2c$ respectively, and it has a unit thickness. When the beam is under end shear load, the following exact solution is given in [Timoshenko and Goodier (1970)]:

$$\begin{aligned}
u_x &= -\frac{Py}{6\overline{E}I}[3x(2L-x)+(2+\overline{\nu})(y^2-c^2)] \\
u_y &= \frac{P}{6\overline{E}I}[x^2(3L-x)+3\overline{\nu}(L-x)y^2+(4+5\overline{\nu})c^2x] \\
\sigma_x &= -\frac{P}{I}(L-x)y \\
\sigma_y &= 0 \\
\sigma_{xy} &= -\frac{P}{2I}(y^2-c^2)
\end{aligned} \tag{83}$$

When the beam is under end bending moment, the following exact solution can also be found:

$$\begin{aligned}
u_x &= -\frac{M}{\overline{E}I}xy \\
u_y &= \frac{P}{2\overline{E}I}(x^2+\overline{\nu}y^2) \\
\sigma_x &= -\frac{M}{I}y \\
\sigma_y &= -\frac{\nu}{1-\nu^2}\frac{M}{I}y \\
\sigma_{xy} &= 0
\end{aligned} \tag{84}$$

where

$$\begin{aligned}
I &= \frac{2c^3}{3} \\
\overline{E} &= \begin{cases} E & \\ E/(1-\nu)^2 & \end{cases} \qquad \overline{\nu} = \begin{cases} \nu & \text{for plane stress} \\ \nu/(1-\nu) & \text{for plane strain} \end{cases}
\end{aligned} \tag{85}$$

The first problem using this beam model is to test the overall performance of these elements against locking, with slightly distorted elements, as used in [Pian and Sumihara (1984)], see Fig 6. Plane stress case is considered with geometry properties $L = 10$, $c = 1$, material properties $E = 1500$ and $\nu = 0.25$. Two loading cases

are considered: end shear load $P = 300$ and end bending moment $M = 2000$. Computed tip vertical displacement at point A, and normal stress at lower left Gaussian point B of the leftmost element are shown in Tab. 5. One can see that severe locking exists for DPFEM, which has great influence on both deflection and stress. HMFEM1-a,b and HMFEM2-a,b in general perform much better, especially for normal stress. For this particular problem, HMFEM2-a seems to have the best performance.

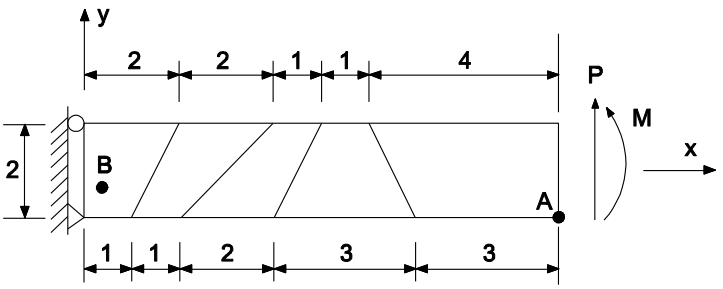

Figure 6: Mesh configuration for overall test of performance against locking

Table 5: Computed and exact solution of cantilever beam in Fig. 6 under end shear or bending moment

Element Type	End Shear		End Bending	
	v_A	σ_B	v_A	σ_B
DPFEM-Q4	49.9	1597.5	44.9	1101.7
HMFEM1-a	70.9	2187.4	66.6	1533.7
HMFEM1-b	66.8	2102.2	62.4	1464.0
HMFEM2-a	77.8	2214.8	73.3	1559.8
HMFEM2-b	66.7	2102.1	62.3	1463.9
Exact	102.6	2531.6	100.3	1732.1

The second problem using this beam model is to test the sensitivity of different methods to mesh distortion, as used in [Punch and Atluri (1984)]. Plane stress case is considered with geometry $L = 10$, $c = 1$, material properties $E = 1.0$ and $v = 0$. The distortion ratio is defined as e/L, as can be seen in Fig. 7. Computed vertical displacement is evaluated at tip point A, and normal stress is evaluated at the lower left Gauss point B (2 by 2 rule) of the leftmost element. The computed results are compared to exact solutions, and plotted in Fig. 8-9, with an end unit

shear load. When the beam is subject to end unit bending moment, computational results are evaluated at the same points, and plotted in Fig. 10-11. As can be clearly seen in Fig. 8-11, DPFEM-Q4 is always performing badly because of locking. HMFEM1-a,b and HMFEM2-a,b all perform similarly. These hybrid/mixed elements can produce almost the exact solution at first, but they are all stiffened along with mesh distortion. However, compared to vertical displacement, normal stresses of HMFEM1-a,b and HMFEM2-a,b are much less sensitive to mesh distortion.

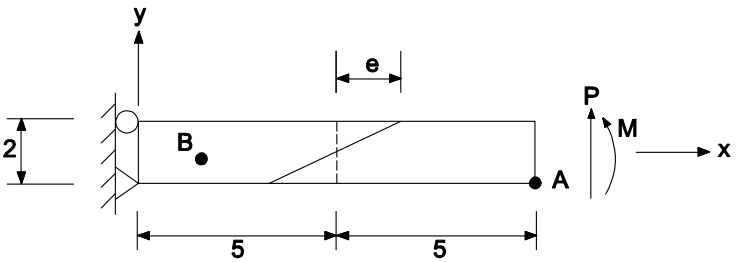

Figure 7: Test of element sensitivity to distortion, cantilever beam under end loading

The cantilever beam problem is finally solved to compare convergence rates of different elements. Plane stress case with geometrical properties $L = 24$, $c = 2$, material properties $E = 1$ and $v = 0.25$ are used as in [Atluri, Han and Rajendran (2004)]. Regular uniform square-shaped elements are used in order to simply compare convergence rates. Nodal distances of 2.0, 1.0 and 0.5 are used, as shown in Fig. 12. The numbers of elements are 24, 96 and 384 respectively. Vertical displacement is evaluated at tip point A, and normal stress is evaluated at lower left corner B. Relative errors of computed solutions of different methods are plot in Fig. 13-16. As can be clearly seen, HMFEM1-a,b, HMFEM2-a,b and DPFEM-Q4 have almost the same good convergence rate. However, under same mesh configuration, the relative errors produced by HMFEM1-a,b and HMFEM2-a,b are almost an order less than DPFEM, because of their ability to avoid locking.

According to the results shown in section 6.1 - 6.3, we see that HMFEM1-a,b HMFEM2-a,b have similar yet much better performance than DPFEM-Q4, in terms of the ability to pass the constant strain patch test, sensitivity to mesh distortion, locking, and convergence rates. Because HMFEM2-b is the most efficient hybrid/mixed element in computation, and do not involve LBB conditions, we consider HMFEM2-b to be the best element for engineering applications.

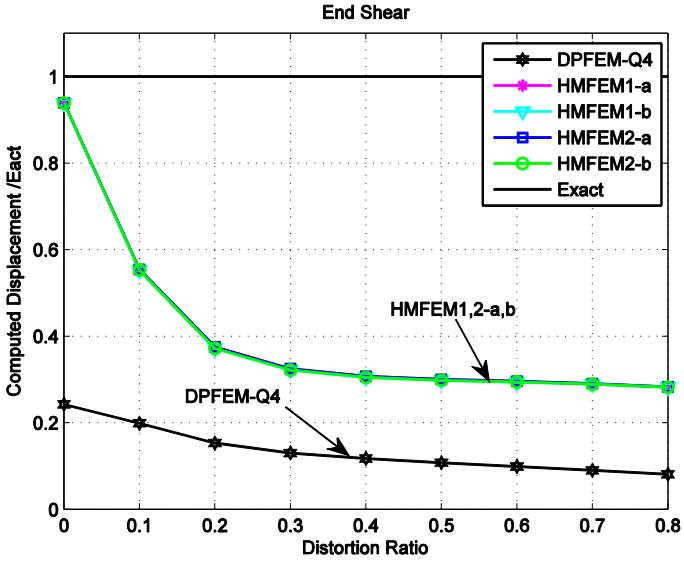

Figure 8: Computed vertical displacement of cantilever beam in Fig. 7 under end shear

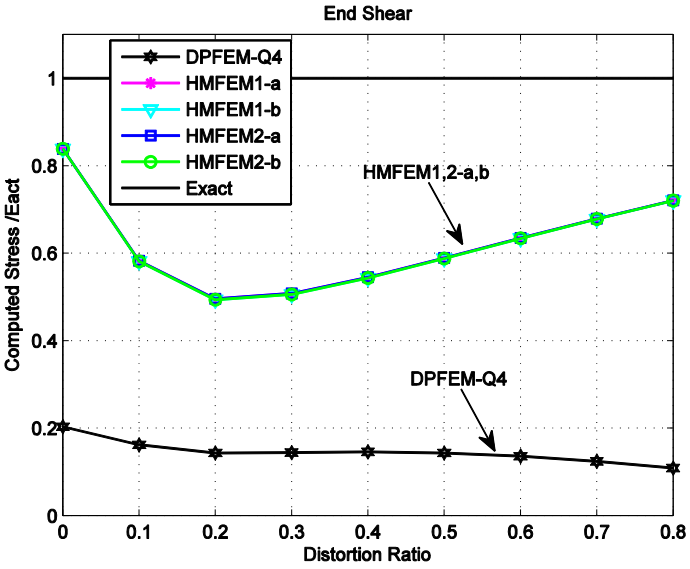

Figure 9: Computed normal stress of cantilever beam in Fig. 7 under end shear

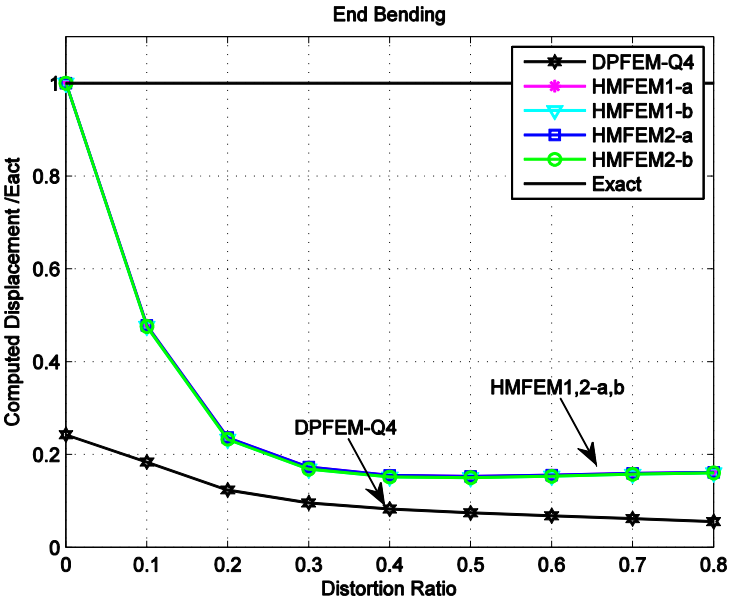

Figure 10: Computed vertical displacement of cantilever beam in Fig. 7 under end bending

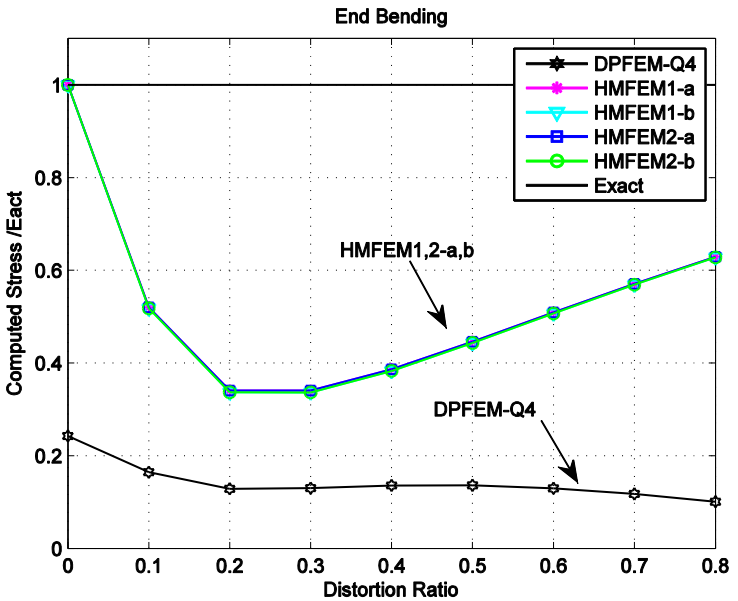

Figure 11: Computed normal stress of cantilever beam in Fig. 7 under end bending

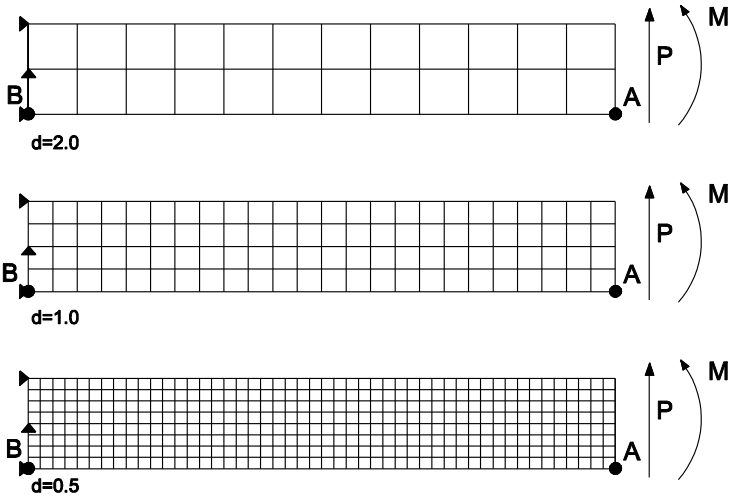

Figure 12: Three meshing configurations of the cantilever beam for test of convergence

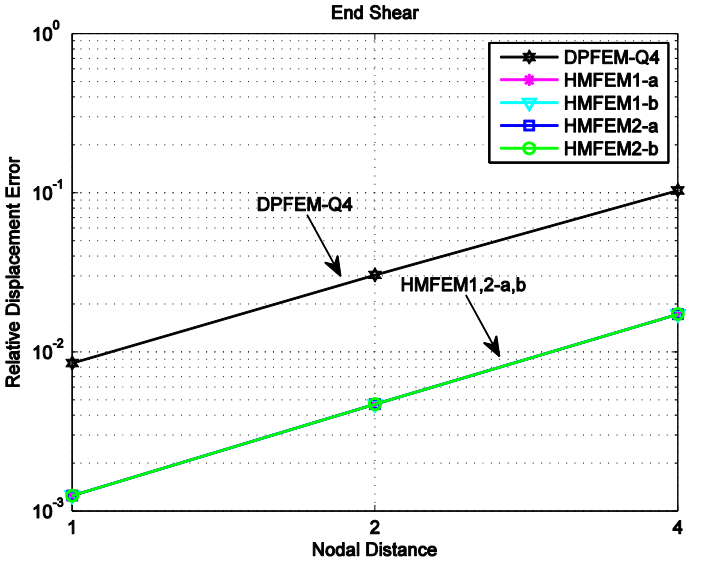

Figure 13: Convergence rate of vertical displacement of cantilever beam in Fig. 12 under end shear

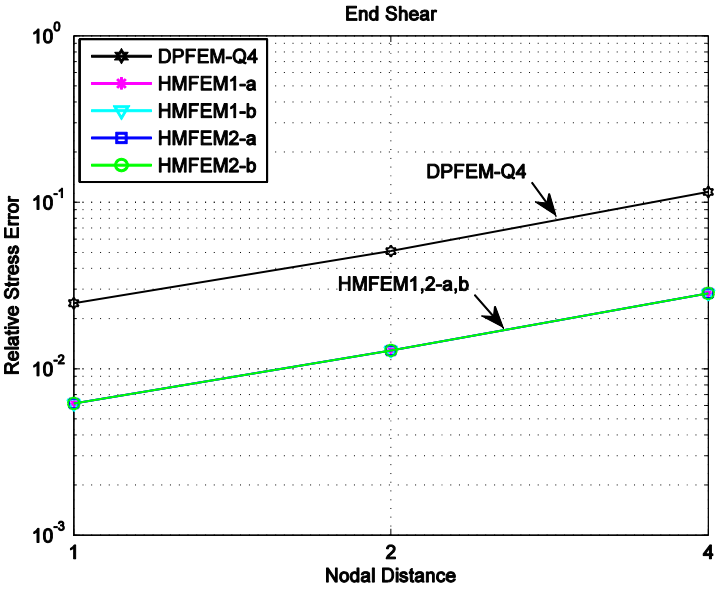

Figure 14: Convergence rate of normal stress of cantilever beam in Fig. 12 under end shear

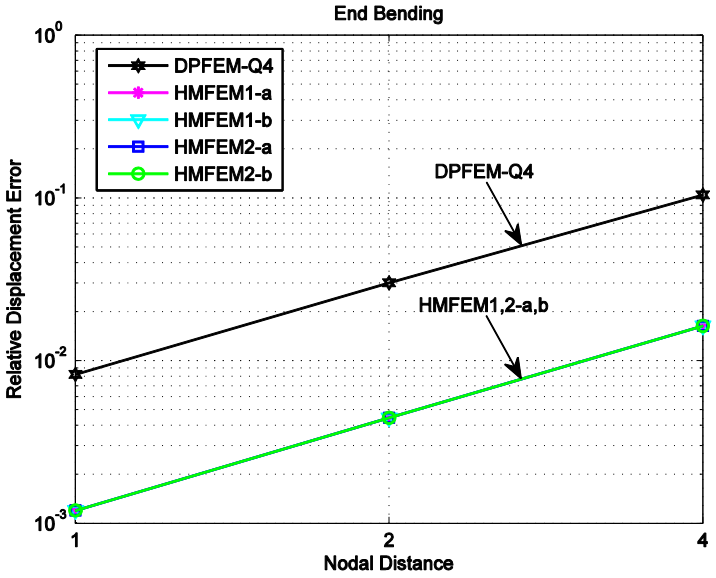

Figure 15: Convergence rate of vertical displacement of cantilever beam in Fig. 12 under end bending

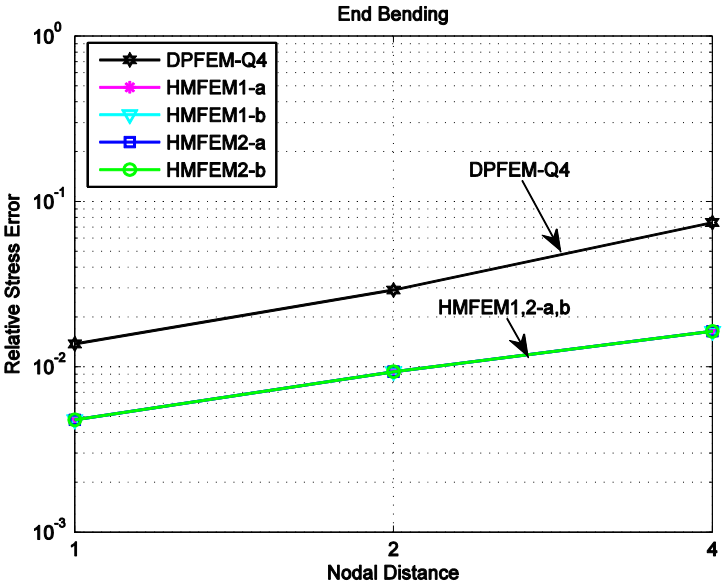

Figure 16: Convergence rate of normal stress of cantilever beam in Fig. 12 under end bending

6.4 Numerical Examples for VCFEMs

In this section, we demonstrate numerical experiments for VCFEMs. In this study, both VCFEM-RBF1 and VCFEM-RBF2 use 8 RBF center/collocations located at Gaussian integration points on each edge. The support size of each RBF is defined as the longest distance to other RBF centers. All results for VCFEM-RBF1,2 are compared to that for VCFEM-HS. The stress field assumption used for VCFEM-HS in this study is complete Airy stress functions, as used in [Ghosh and Mallett (1994)].

Firstly, we carry out eigenvalue analysis of for VCFEMs, similarly to what was done in section 6.1. Plane stress problem with $E = 1$ and $v = 0.25$ are considered. A regular pentagon and a regular hexagon with unit radius are used, see Fig. 17. of VCFEM-RBF1,2 and VCFEM-HS are calculated in the original Cartesian coordinate system. CPU time used for computing the stiffness matrix of each pentagon element is also shown in Tab. 8. Then the coordinate system is rotated counter-clockwise by 45˚, of these elements are calculated again. Eigenvalues of these element stiffness matrices are demonstrated in Tab. 6 and Tab. 7.

As can clearly be seen, these elements are stable and invariant, because only 3 zero

eigenvalues exist for each element, and eigenvalues do not change with respect to change of coordinate system. The smallest eigenvalue of elements for VCFEM-RBF1,2 are larger than that for VCFEM-HS, which means better element stability. Moreover, as shown in Tab. 8, derivation of element stiffness matrices of VCFEM-RBF1,2 requires less computational burden than that for VCFEM-HS.

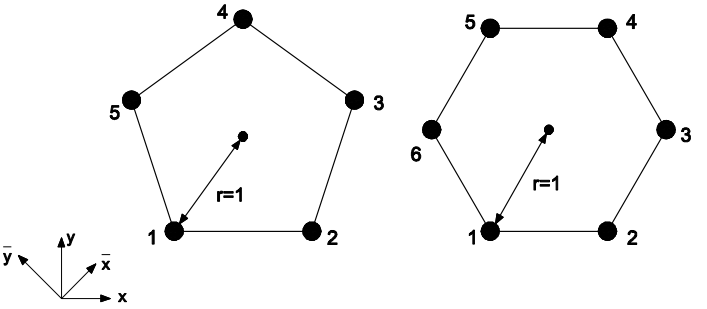

Figure 17: A pentagon and a hexagon element

Secondly, we conduct the constant strain patch test. The same problem as shown in section 6.2 is solved, with mesh configuration shown in Fig. 18. The errors defined as in (82) for VCFEM-RBF1,2 and VCFEM-HS are demonstrated in Tab. 9. Although VCFEM-RBF1,2 cannot theoretically exactly reproduce the linear field as VCFEM-HS, very small errors are produced for both VCFEM-RBF1 and VCFEM-RBF2.

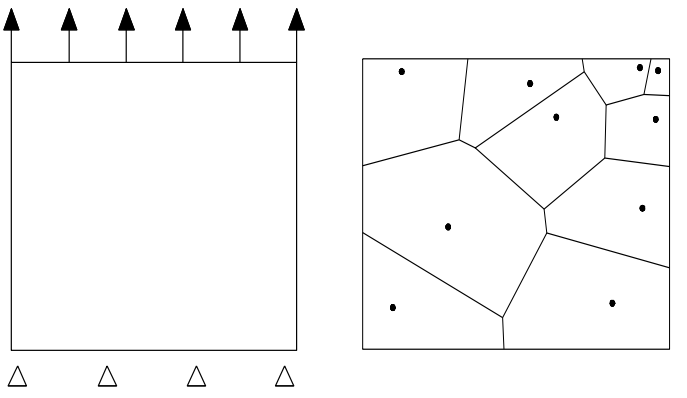

Figure 18: Mesh configuration used for the constant strain patch test of VCFEMs

Table 6: Eigenvalues of stiffness matrices of pentagon elements

Eigenvalue Number	VCFEM-RBF1		VCFEM-RBF2		VCFEM-HS	
	Rotation =0°	Rotation =45°	Rotation =0°	Rotation =45°	Rotation =0°	Rotation =45°
1	1.2681	1.2681	1.2681	1.2681	1.2681	1.2681
2	0.7608	0.7608	0.7608	0.7608	0.7608	0.7608
3	0.7608	0.7608	0.7608	0.7608	0.7608	0.7608
4	0.6721	0.6721	0.5389	0.5389	0.5751	0.5751
5	0.6721	0.6721	0.5389	0.5389	0.5751	0.5751
6	0.5934	0.5934	0.3814	0.3814	0.2614	0.2614
7	0.5934	0.5934	0.3814	0.3814	0.2614	0.2614
8	0.0000	0.0000	0.0000	0.0000	0.0000	0.0000
9	0.0000	0.0000	0.0000	0.0000	0.0000	0.0000
10	0.0000	0.0000	0.0000	0.0000	0.0000	0.0000

Table 7: Eigenvalues of stiffness matrices of hexagon elements

Eigenvalue Number	VCFEM-RBF1		VCFEM-RBF2		VCFEM-HS	
	Rotation =0°	Rotation =45°	Rotation =0°	Rotation =45°	Rotation =0°	Rotation =45°
1	1.1547	1.1547	1.1547	1.1547	1.1547	1.1547
2	0.8163	0.8163	0.6928	0.6928	0.7390	0.7390
3	0.7644	0.7644	0.6928	0.6928	0.7390	0.7390
4	0.6928	0.6928	0.6642	0.6642	0.6928	0.6928
5	0.6928	0.6928	0.6330	0.6330	0.6928	0.6928
6	0.6744	0.6744	0.4521	0.4521	0.4783	0.4783
7	0.6744	0.6744	0.4521	0.4521	0.4783	0.4783
8	0.6217	0.6217	0.4427	0.4427	0.3359	0.3359
9	0.6217	0.6217	0.3907	0.3907	0.3359	0.3359
10	0.0000	0.0000	0.0000	0.0000	0.0000	0.0000
11	0.0000	0.0000	0.0000	0.0000	0.0000	0.0000
12	0.0000	0.0000	0.0000	0.0000	0.0000	0.0000

Table 8: CPU time required for computing the stiffness matrix of each VCFEM pentagon element, normalized to that for VCFEM-HS element.

CPU Time	Elements		
	VCFEM-RBF1	VCFEM-RBF2	VCFEM-HS
	0.76	0.81	1.00

Table 9: Performances of different VCFEMs in the constant strain patch test

Element	VCFEM-RBF1	VCFEM-RBF2	VCFEM-HS
Error	4.6×10^{-4}	8.8×10^{-4}	8.8×10^{-10}

Finally, we evaluate the performance of VCFEMs by modeling the cantilever beam as shown in Fig. 19, and compare their performances to the exact solution. Plane stress situation is considered with geometry properties $L = 10$, $c = 1$, material properties $E = 1500$ and $v = 0.25$. Two loading cases are considered: end shear load $P = 300$ and end bending moment $M = 2000$. The mesh configuration includes 10 elements. Computed tip vertical displacement at point A, and normal stress at lower left corner are shown in Tab. 10. The results are consistent with our previous analysis. While both elements give acceptable results, VCFEM-RBF2 demonstrates better performance than VCFEM-RBF1. This is because VCFEM-RBF1 suffers from locking, while VCFEM-RBF2 is able to avoid locking by eliminating the shear locking terms in its independently assumed strains. In addition, VCFEM-RBF2 performs similarly to VCFEM-HS, for this particular problem. VCFEM-RBF2 gives slightly more accurate vertical displacements, but slightly less accurate normal stresses.

From numerical results shown in this section, we see that VCFEM-RBF2 have similar element performance to VCFEM-HS, in terms of accuracy of solution. However, VCFEM-RBF2 is computationally more efficient than VCFEM-HS. Moreover, selection of "a priori equilibrated", independent and invariant stress field, which satisfies LBB conditions a priori for VCFEM-HS, is especially difficult for elements with a large number of edges, and impossible for geometrical nonlinear and dynamical problems. Therefore, we consider VCFEM-RBF2 more suitable for engineering applications, and its extension to three-dimensional problems will be studied in future.

7 Conclusion

A simple procedure to formulate hybrid/mixed finite elements is developed for applications in macro- as well as micromechanics of solids. In this approach, inde-

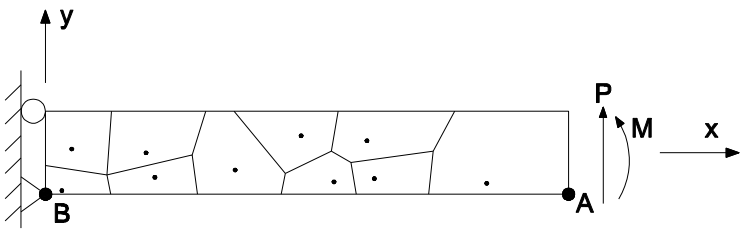

Figure 19: Mesh configuration used for overall test of performances of VCFEMs

Table 10: Computed and exact solution of cantilever beam in Fig. 19 under end shear or bending moment

Element Type	End Shear		End Bending	
	v_A	σ_B	v_A	σ_B
VCFEM-RBF1	78.0	3320.3	74.0	2354.8
VCFEM-RBF2	90.9	3781.0	86.7	2643.9
VCFEM-HS	89.6	3844.0	86.4	2696.8
Exact	102.6	4500	100.3	3000

pendently assumed strains in each element are related to the strains derived from independently assumed displacements, at a finite number of collocation points within the element. The element stiffness matrix is thereafter developed, by simply using the principle of minimum potential energy. In addition to their self-explanatory efficiency, the developed elements are also guaranteed to be stable, because no LBB conditions are involved. By adopting different assumptions of strain field and using different collocation points in a plane four-node isoparametric element, different elements are developed. Compared to traditional four-node isoparametric primal and hybrid/mixed elements in a series of numerical examples, we can clearly see the advantages of the current approach. Among all the elements, we highly recommend HMFEM2-b, because it is invariant, stable, locking-free, less sensitive to mesh-distortion, and computationally most efficient, with only trivial changes to the DPFEM-Q4 element. Elements similar to HMFEM2-b in higher-order and higher-dimension is also recommended, which are expected to have good element performances.

We point out that this procedure can be used to develop hybrid/mixed elements for applications in other physical problems. We also extend this idea to develop Voronoi cell finite elements. Two VCFEMs are developed, named VCFEM-RBF1 and VCFEM-RBF2, which are invariant, efficient, and do not involve LBB condi-

tions. VCFEM-RBF2 is also locking-free, because of its independently assumed unlocked strains. Moreover, because there is no need to select "a priori equilibrated" stress field, VCFEM-RBF1,2 can be easily extended to solve geometrical nonlinear and dynamical problems, which is a significant advantage compared to VCFEMs proposed by [Ghosh and his co-workers (1994, 1995 and many more in the past 20 years)].

Acknowledgement: This paper is an outcome of the homework assigned in the course MAE 207, taught in spring 2011 by the second author at University of California, Irvine (UCI). This work was also supported in part by the Vehicle Technology Division of the Army Research labs, under a collaborative research agreement with UCI, and in part by the Word Class University (WCU) program through the National Research Foundation of Korea, funded by the Ministry of Education, Science and Technology (Grant no.: R33-10049). The first author also would like to thank Professor Masanobu Shinozuka for his kind support of the first author's study.

References

Atluri, S. N. (1975): On hybrid finite element models in solid mechanics. *Advances in Computer Methods* for *Partial Differential Equations,* R. Vichnevetsky (eds.), AICA, pp. 346-356.

Atluri, S. N.; Tong, P.; Murakawa, H. (1983): Recent studies in hybrid and mixed finite element methods in mechanics. *Hybrid and Mixed Finite Element Methods*, S.N. Atluri, R.H. Gallagher and O.C. Zienkiewicz (eds.), pp. 51-71.

Atluri, S. N.; Han, Z. D.; Rajendran, A. M. (2004): A new implementation of the meshless finite volume method, through the MLPG "mixed" approach. *CMES: Computer Modeling in Engineering & Sciences*, vol. 6, no. 6, pp. 491–514.

Atluri, S.N. (2005): *Methods of Computer Modeling in Engineering and the Sciences, Vol. 1*, Tech Science Press.

Avila, R; Han, Z. D.; Atluri, S. N. (2011): A novel MLPG-finite-volume mixed method for analyzing Stokesian flows & study of a new vortex mixing flow. *CMES: Computer Modeling in Engineering & Sciences, vol. 71, no. 4, pp. 363-396.*

Babuska, I (1973): The finite element method with Lagrangian multipliers. *Numerische Mathematik*, vol. 20, no. 3, pp. 179-192.

Bicanic, N.; Hinton, E. (1979): Spurious modes in two-dimensional isoparametric elements. *International Journal for Numerical Methods in Engineering*, vol. 14, issue 10, pp. 1545–1557.

Bratianu, C.; Atluri, S. N. (1983): A hybrid finite element method for Stokes flow: part I-formulation and numerical studies. *Computer Methods in Applied Mechanics and Engineering*, vol. 36, pp. 23–37.

Brezzi, F. (1974): On the existence, uniqueness and approximation of saddle-point problems arising from Lagrangian multipliers. *Revue Française D'automatique, Informatique, Recherche Opérationnelle, Analyse Numérique*, vol. 8, no. 2, pp. 129-151.

Cai, Y. C.; Paik, J. K.; Atluri, S. N. (2009): Large deformation analyses of space-frame structures, with members of arbitrary cross-section, using explicit tangent stiffness matrices, based on a von Karman type nonlinear theory in rotated reference frames, *CMES: Computer Modeling in Engineering & Sciences*, vol. 53, no. 2, pp. 117-145.

Cai, Y. C.; Paik, J. K.; Atluri, S. N. (2009): Large deformation analyses of space-frame structures, using explicit tangent stiffness matrices, based on the Reissner variational principle and a von Karman type nonlinear theory in rotated reference frames. *CMES: Computer Modeling in Engineering & Sciences*, vol. 54, no. 3, pp. 335-368.

Cai, Y. C.; Paik, J. K.; Atluri, S. N. (2010): Locking-free thick-thin rod/beam element for large deformation analyses of space-frame structures, based on the Reissner variational principle and a von Karman type nonlinear theory, *CMES: Computer Modeling in Engineering & Sciences*, vol. 58, no. 1, pp. 75-108.

Cai, Y. C.; Paik, J. K.; Atluri, S. N. (2010): A triangular plate element with drilling degrees of freedom, for large rotation analyses of built-up plate/shell structures, based on the Reissner variational principle and the von Karman nonlinear theory in the co-rotational reference frame. *CMES: Computer Modeling in Engineering & Sciences*, vol. 61, no. 3, pp. 273-312.

Cazzani, A.; Garusi, E.; Tralli, A.; Atluri, S. N. (2005): A four-node hybrid assumed-strain finite element for laminated composite plates. CMC: *Computers, Materials & Continua*, vol. 2, no. 1, pp. 23-38.

Ghosh, S.; Mallett, R. L. (1994): Voronoi cell finite elements. *Computers & Structures*, vol. 50, issue 1, pp. 33-46.

Ghosh, S.; Lee, K; Moorthy, S. (1995): Multiple scale analysis of heterogeneous elastic structures using homogenization theory and Voronoi cell finite element method. *International Journal of Solids and Structures*, vol. 32, issue 1, pp. 27-63.

Golberg, M. A., Chen, C. S., Bowman, H. (1999)**:** Some recent results and proposals for the use of radial basis functions in the BEM, *Engineering Analysis with Boundary Elements*, vol. 23, pp. 285-296.

Lee, S. W.; Pian, T. H. H. (1978): Improvement of plate and shell finite elements by mixed formulations. *A. I. A. A. Journal*, vol. 16, issue 1, pp. 29-34.

Pian, T. H. H. (1964): Derivation of element stiffness matrices by assumed stress distribution. *A. I. A. A. Journal*, vol. 2, pp. 1333-1336.

Pian, T. H. H., Mau, S. T. (1972): Some recent studies in assumed stress hybrid models. *Advances in Computational Methods in Structural Mechanics and Design*, Oden, Clought, Yamamoto (eds.), pp. 87-106.

Pian, T. H. H.; Chen, D. (1983): On the suppression of zero energy deformation modes. *International Journal for Numerical Methods in Engineering*, vol. 19, issue 12, pp. 1741–1752.

Pian, T. H. H.; Wu, C. (1983): A rational approach for choosing stress terms for hybrid finite element formulations. *International Journal for Numerical Methods in Engineering*, vol. 26, issue 10, pp. 2331–2343.

Pian, T. H. H.; Sumihara, K. (1984): Rational approach for assumed stress finite elements. *International Journal for Numerical Methods in Engineering*, vol. 20, issue 9, pp. 1685–1695.

Punch, E. F.; Atluri, S. N. (1984): Development and testing of stable, invariant, isoparametric curvilinear 2- and 3-D hybrid-stress elements. *Computer Methods in Applied Mechanics and Engineering*, vol 47, issue 3, pp. 331-356.

Reissner, E. (1950): On a variational theorem in elasticity. *Journal of Mathematical Physics*, vol. 29, pp. 90-95.

Rubinstein, R.; Punch, E. F.; Atluri, S. N. (1984): An analysis of, and remedies for, kinematic modes in hybrid-stress finite elements: selection of stable, invariant stress fields. *Computer Methods in Applied Mechanics and Engineering*, vol. 38, issue 1, pp. 63-92.

Spilker, R. L.; Maskeri, S. M.; Kania, E. (1981): Plane isoparametric hybrid-stress elements: invariance and optimal sampling. *International Journal for Numerical Methods in Engineering*, vol. 17, issue 10, pp. 1469–1496.

Sze, K. Y.; Chow, C. L.; Chen, W. (1992): On invariance of isoparametric hybrid/mixed elements. *Communications in Applied Numerical Methods*, vol. 8, issue 6, pp. 385–406.

Tang, L.; Chen, W.; Liu, Y. (1984): Formulation of Quasi-Conforming element and Hu-Washizu principle. *Computers & Structures*, vol. 19, issue 1-2, pp. 247-250.

Timoshenko, S. P.; Goodier, J. N. (1976): *Theory of Elasticity*, 3^{rd} edition, McGraw Hill.

Wu, Z (1995): Compactly supported positive definite radial functions. *Advances*

in Computational Mathematics, vol. 4, no. 1, pp. 283-292.

Xue, W.; Karlovitz, L. A.; Atluri, S. N. (1985): On the existence and stability conditions for mixed-hybrid finite element solutions based on Reissner's variational principle. *International Journal of Solids and Structures*, vol. 21, issue 1, 1985, pp. 97-116.

Ying, L. A.; Atluri, S. N. (1983): A Hybrid finite element method for Stokes flow: Part II-stability and convergence studies. *Computer Methods in Applied Mechanics and Engineering*, vol. 36, pp. 39–60.

Zhu, H. H.; Cai, Y.C.; Paik, J.K.; Atluri, S. N. (2010): Locking-free thick-thin rod/beam element based on a von Karman type nonlinear theory in rotated reference frames for large deformation analyses of space-frame structures. *CMES: Computer Modeling in Engineering & Sciences*, vol. 57, no. 2, pp. 175-204.